Optimal Energy Signal Design for Multiuser MISO WPCNs With Non-Linear Energy Harvesting Circuits

Nikita Shanin, *Graduate Student Member, IEEE*, Amelie Hagelauer, *Senior Member, IEEE*, Laura Cottatellucci, *Member, IEEE*, and Robert Schober, *Fellow, IEEE*

***Abstract*— The optimal energy signal design for wireless powered communication networks (WPCNs) enabling energy-sustainable communication for a large number of low-power devices is still an open problem in practical systems. In this work, we study a multi-user WPCN, where a multi-antenna base station (BS) sends an energy signal to multiple single-antenna users, which, in turn, harvest energy from the received signal and utilize it for information transmission in the uplink. In contrast to the existing works on multiple-input single-output (MISO) WPCN design, in this paper, we jointly optimize the energy signal waveform and downlink beamforming at the BS for energy harvesting (EH) devices described by non-linear circuit-based models. To this end, we assume that the BS broadcasts a pulse-modulated signal employing multiple energy signal vectors and we formulate an optimization problem for the joint design of the downlink transmit energy signal vectors, their number, the durations of the transmit pulses, and the time allocation policy for minimization of the average transmit power at the BS. We show that for single-user WPCNs, a single energy signal vector, which is collinear with the maximum ratio transmission (MRT) vector and drives the EH circuit at the user device into saturation, is optimal. Next, for the general multi-user case, we show that the optimal signal design requires a maximum number of energy signal vectors that exceeds the number of users by one and propose an algorithm to obtain the optimal energy signal vectors. Since the complexity of the optimal design is high, we also propose two suboptimal schemes for WPCN design. First, for asymptotic massive WPCNs, where the ratio of the number of users to the number of BS antennas, i.e., the system load, tends to zero, we show that the optimal downlink transmit signal can be obtained in closed-form and comprises a sequence of weighted sums of MRT vectors. Next, based on this result, for general WPCNs with finite system loads, we propose a suboptimal closed-form MRT-based design and a suboptimal semidefinite relaxation (SDR)-based scheme. Our simulation results reveal that the proposed optimal scheme and suboptimal SDR-based design achieve nearly identical performance and outperform two baseline schemes, which are based on linear and sigmoidal EH models. Furthermore, we show that, if the system load of the WPCN is low, the performance gap between the proposed suboptimal solutions is small and becomes negligible as the number of BS antennas tends to infinity.**

***Index Terms*— Wireless powered communication, non-linear energy harvesting, multiple-input multiple-output (MIMO), signal design.**

Manuscript received 18 August 2022; revised 5 January 2023 and 13 February 2023; accepted 7 March 2023. Date of publication 15 March 2023; date of current version 16 June 2023. This work was supported in part by the German Science Foundation through project SFB 1483 - Project-ID 442419336, EmpkinS. An earlier version of this paper was presented at the IEEE International Conference on Acoustics, Speech and Signal Processing (ICASSP), Singapore, 2022 [DOI: 10.1109/ICASSP43922.2022.9747494]. The associate editor coordinating the review of this article and approving it for publication was B. Shim. *(Corresponding author: Nikita Shanin.)*

Nikita Shanin, Laura Cottatellucci, and Robert Schober are with the Institute for Digital Communications, Friedrich-Alexander-Universität (FAU) Erlangen-Nürnberg, 91058 Erlangen, Germany (e-mail: nikita.shanin@fau.de; laura.cottatellucci@fau.de; robert.schober@fau.de).

Amelie Hagelauer is with the Chair of Micro and Nanosystems Technology, Technische Universität München, 85748 Munich, Germany, and also with the Fraunhofer Institute for Electronic Microsystems and Solid State Technologies EMFT, 80686 Munich, Germany (e-mail: amelie.hagelauer@tum.de).

Color versions of one or more figures in this article are available at https://doi.org/10.1109/TCOMM.2023.3257379.

Digital Object Identifier 10.1109/TCOMM.2023.3257379

I. Introduction

THE growth of the number of low-power Internet-of-Things (IoT) devices has fuelled significant interest in wireless powered communication networks (WPCNs) that enable energy-sustainable communication [1], [2], [3], [4], [5], [6], [7], [8], [9], [10], [11], [12], [13], [14], [15], [16], [17], [18], [19], [20], [21], [22], [23], [24], [25]. A typical multi-user multiple-input single-output (MISO) WPCN comprises a multi-antenna base station (BS) that broadcasts a radio frequency (RF) signal to multiple single-antenna user devices (e.g., small-scale biomedical sensors or implants) in the downlink [2]. Each user device is equipped with an electrical circuit for harvesting the received RF power and storing it in a supercapacitor or a storage battery. The user devices employ the harvested power for sensing, signal processing and operational tasks, and information transmission in the uplink [3]. Thus, such a low-power equipment can not only communicate with the BS, but also recharge energy storage devices, whose periodic replacement may be costly or even impossible [4], [5].

For the design of WPCNs, a linear relationship between the received and harvested powers at the user devices is assumed in [6], [7], [8], [9], and [10]. In [6], for multi-user single-input single-output (SISO) WPCNs, the authors formulate a sum-throughput maximization problem and unveil a *double-near-far* phenomenon resulting in an uneven rate allocation among the users. To ensure reliable uplink communication, the authors in [6] also considered a minimum-throughput maximization problem and showed that, due to the distance-dependent signal attenuation, the BS has to allocate significantly more resources in the downlink to far users compared to

near users. Next, in [7], the authors study multi-user WPCNs, where the BS employs multiple antennas and utilizes zero forcing (ZF) equalization to suppress the inter-user interference in the uplink. For this setup, the authors propose an algorithm for downlink energy beamforming that maximizes the minimum information rate in the uplink. The authors in [8] study a massive multiple-input multiple-output (MIMO) WPCN and show that the optimal energy beamforming in the downlink is a linear combination of the normalized channel vectors between the BS and the user devices. In [9], the authors consider multi-user WPCNs, where time division multiple access (TDMA) is adopted for information transmission in the uplink and users are equipped with infinite or finite capacity energy storage. It is shown that the optimal transmit policy at the BS is to radiate all available power as fast as possible, and then, remain silent until the end of the scheduling time frame. The energy storage at the user devices of a WPCN is further considered in [10]. In this paper, the authors characterize the internal state of the energy buffer via a Markov chain and, for Rayleigh fading channels, determine the limiting distribution of the stored power in closed-form.

Although the results in [6], [7], [8], [9], and [10] provide notable insights for WPCN design, they are based on restrictive impractical assumptions. In fact, practical energy harvesting (EH) circuits employ non-linear diodes for signal rectification and thus, the dependence of the harvested power on the input power is highly non-linear in both the low and high input power regimes [4], [11]. If the received RF power at a user device is low, the non-linearity is caused by both the non-linear current-voltage (I-V) characteristic of the rectifying diode [12] and the power-dependent impedance mismatch between the receive antenna and the non-linear rectifier circuit [13]. For high input powers, the non-linear diode is driven into breakdown, which causes saturation of the harvested power at the user device [3]. To take these non-linear effects of the EH circuits into account, the authors in [14] propose a sigmoid function-based EH model, whose parameters are obtained via curve fitting to match simulation data. This model is widely employed for the design of WPCNs, see, e.g., [15], [16], [17], [18], and [19]. In particular, the authors in [15] study multi-user MIMO WPCNs, where, similarly to [9], a TDMA scheme is employed for information transfer in the uplink. In [16], the authors consider a wireless communication system, where a wirelessly charged multi-antenna BS transmits information to multiple single-antenna receivers in the presence of an eavesdropper. Furthermore, the authors in [17], [18], and [19] study WPCNs assisted by intelligent reflecting surfaces, which are employed to increase the harvested powers at the user devices, and thus, improve the overall uplink throughput. For the considered system setups, the authors in [15], [16], [17], [18], and [19] formulate non-convex resource allocation optimization problems for system design and propose iterative algorithms to solve them.

The analysis in [15], [16], [17], [18], and [19] represents a significant progress over the results in [6], [7], [8], [9], and [10]. However, the model introduced in [14] and adopted in [15], [16], [17], [18], and [19] characterizes the *average* harvested power at the user devices as a function of the *average* received RF power, and therefore, cannot fully capture the non-linearity of EH circuits. Interestingly, the authors in [20] propose an EH model that maps the *instantaneous* received RF power to the *instantaneous* harvested power. Based on this EH model, the author in [21] considers single-user wireless power transfer systems and shows that the power harvested at the user is maximized if maximum ratio transmission (MRT) is adopted at the multi-antenna BS in the downlink. Furthermore, the EH model in [20] is utilized in [22] and [23] for the analysis of backscatter communication systems which are also based on wireless power transfer. In particular, the authors in [22] highlight a trade-off between the harvested power at the user device and the signal-to-noise ratio (SNR) of the communication link between user and information receiver. In [23], the authors extend the communication system in [22] to the multi-user case and formulate an optimization problem to analyze the trade-off between the weighted sum of harvested powers at the user devices and the signal-to-interference-plus-noise ratios (SINRs) of the communication links between the users and the receiver.

In contrast to the linear and sigmoidal models in [6], [7], [8], [9], and [10] and [14], [15], [16], [17], [18], and [19], respectively, the EH model in [20] characterizes the instantaneous behaviour of the EH circuits and thus, allows the optimization of the transmit signal waveform for wireless power transfer. However, since this model is based on the Taylor series approximation of the current flow through the rectifying diode and does not take into account the breakdown effect of the diode, it still does not fully capture all non-linear effects of practical EH circuits for both low and high input powers. To overcome this limitation, the authors in [25] propose an EH model based on a precise analysis of a standard EH circuit with half-wave rectifier and show that On-Off transmission is optimal for the maximization of the average harvested power in single-antenna wireless power transfer systems. Next, since the circuit-based model in [25] is valid for half-wave rectifying EH circuits only, the authors in [13] propose a learning-based approach to model a wide class of EH circuits and show that the behaviour of an EH circuit depends on the number of rectifying diodes, the characteristics of the matching circuit, and other circuit parameters. The authors in [24] study a multi-user MIMO wireless power transfer system with general non-linear EH circuits. They design the optimal energy signal to be transmitted by the BS to maximize a weighted sum of the average harvested powers at the EH nodes and show that it comprises multiple beamforming vectors. Finally, in [1], which is the conference version of this paper, we adopt the EH model from [25] and develop an iterative algorithm for the design of two-user MISO WPCNs. However, to the best of the authors' knowledge, the optimal design of the downlink energy signal waveform and the resource allocation for multi-user MISO WPCNs taking into account all non-linear effects of EH circuits is still an open problem, which is tackled in this paper.

In this paper, we determine the optimal downlink energy signal design and resource allocation policy for multi-user MISO WPCNs, where the single-antenna user devices are equipped with non-linear EH circuits, to minimize the average

transmit power at the BS. In contrast to the WPCN designs in [6], [7], [8], [9], [10], [14], [15], [16], [17], [18], [19], and [20], in this work, to account for the non-linearities of the EH circuits in both the low and high input power regimes, we adopt a general non-linear circuit-based EH model that characterizes the instantaneous harvested power at the user devices. Furthermore, in contrast to the existing works on multi-user WPCNs with multi-antenna BSs, to jointly optimize beamforming and the waveform of the downlink energy signal, we assume that the BS broadcasts a pulse-modulated energy signal employing multiple transmit energy signal vectors. The user devices, in turn, harvest the power from the received RF energy signal and utilize it for information transmission in the uplink, where we adopt ZF equalization at the BS to suppress inter-user interference. The main contributions of this paper can be summarized as follows:

- We formulate an optimization problem for the joint design of the normalized durations of the downlink and uplink transmission subframes and the number, durations, values, and powers of the downlink transmit energy signal vectors for minimization of the average transmit power at the BS under per-user rate constraints in the uplink.
- First, as a special case, we consider a single-user WPCN and show that the optimal energy signal in the downlink employs a single vector, which is collinear with the MRT vector and whose norm is chosen such that it drives the EH circuit at the user device into saturation. Then, for the general multi-user case, we show that the maximum number of transmit energy signal vectors for the optimal signal design in the downlink exceeds the number of users by one. To obtain these energy signal vectors, we propose an optimal algorithm whose computational complexity is exponential in the number of user devices and polynomial in the number of antennas equipped at the BS.
- Since the optimal solution for the general multi-user case entails a high computational complexity if the number of users is large, we also propose two low-complexity suboptimal solutions. First, we show that for asymptotic massive MISO WPCNs, where the ratio of the number of users and number of BS antennas, i.e., the system load, tends to zero, the optimal downlink energy signal comprises a sequence of weighted sums of MRT beamforming vectors and can be obtained in closed-form. Next, based on this result, we design an MRT-based scheme, which is optimal for massive MISO WPCNs with vanishing system loads and provides a suboptimal solution of the formulated problem for general MISO WPCNs with finite system loads. Furthermore, to improve the performance of the MRT-based design for general WPCNs, we derive a low-complexity suboptimal scheme, which is based on semi-definite relaxation (SDR).
- Our simulation results reveal that the proposed SDR-based suboptimal design has a significantly lower computational complexity than the optimal scheme and both WPCN designs achieve nearly identical performance and significantly outperform two baseline schemes, which are based on the linear and sigmoidal EH models, respectively. Also, we show that for low system loads, the proposed suboptimal MRT- and SDR-based schemes have a similar performance and become identical when the number of BS antennas tends to infinity. Finally, we show that when the numbers of deployed BS antennas and user devices grow, the average transmit power in the downlink decreases and increases, respectively.

The remainder of this paper is organized as follows. In Section II, we discuss the proposed system model. In Section III, we formulate the optimization problem for minimizing the average transmit power in the downlink under per-user rate constraints in the uplink, and solve it for the single-user case in closed form. Moreover, for the general multi-user case, we characterize the optimal solution and propose an algorithm to compute it. In Section IV, we consider the asymptotic massive MISO regime and determine a closed-form solution for the resulting optimization problem. Furthermore, for the general non-asymptotic case, we propose two low-complexity suboptimal schemes. In Section V, we evaluate the performance of the proposed framework via numerical simulations. Finally, in Section VI, we draw some conclusions.

Notation: Bold upper case letters $\boldsymbol{X}$ represent matrices and $X_{i,j}$ denotes the element of $\boldsymbol{X}$ in row i and column j. Bold lower case letters $\boldsymbol{x}$ stand for vectors and x_i is the i^{th} element of $\boldsymbol{x}$. $\boldsymbol{X}^H$, $\text{Tr}\{\boldsymbol{X}\}$, and $\text{rank}\{\boldsymbol{X}\}$ denote the Hermitian, trace, and rank of matrix $\boldsymbol{X}$, respectively. $\mathbb{E}\{x\}$ denotes the statistical expectation of x. The real part of a complex number is denoted by $\Re\{\cdot\}$. The transpose and L2-norm of vector $\boldsymbol{x}$ are represented by $\boldsymbol{x}^\top$ and $\|\boldsymbol{x}\|_2$, respectively. The sets of real, real non-negative, and complex numbers are represented by $\mathbb{R}$, $\mathbb{R}_+$, and $\mathbb{C}$, respectively, whereas $\mathcal{S}_+^N$ stands for the set of complex positive semidefinite matrices of size N. $\boldsymbol{X}^{\frac{1}{2}}$ and $\|\boldsymbol{X}\|_2$ stand for the square root and spectral norm of matrix $\boldsymbol{X}$, respectively, whereas $\text{diag}(\boldsymbol{x})$ with $\boldsymbol{x} \in \mathbb{C}^N$ represents a diagonal matrix $\boldsymbol{X} \in \mathbb{C}^{N\times N}$, whose elements are all zero-valued except for $X_{n,n} = x_n, \forall n \in \{1, 2, \cdots, N\}$. The imaginary unit is denoted by j. $f^{-1}(\cdot)$ and $f'(x_0)$ denote the inverse function of $f(\cdot)$ and the first-order derivative of $f(x)$ evaluated at point $x = x_0$, respectively. Generalized non-strict inequalities are denoted by $\succeq$ and $\preceq$ and are associated with $\mathbb{R}_+^N$, i.e., $\forall N \geq 0$ and $\forall \boldsymbol{x}, \boldsymbol{y} \in \mathbb{R}^N$, $\boldsymbol{x} \succeq \boldsymbol{y}$ and $\boldsymbol{y} \preceq \boldsymbol{x} \Longleftrightarrow y_n \leq x_n, \forall n \in \{1, 2, \cdots, N\}$. Furthermore, $\boldsymbol{0}$ and $\boldsymbol{I}_N$ stand for the all-zero vector of appropriate dimension and the identity matrix of size N, respectively.

II. System Model

We consider a single-carrier multi-user MISO WPCN, where $K \geq 1$ single-antenna users are equipped with EH circuits [25] and information transmitters and $N_{\text{t}} \geq K$ antennas are deployed at the BS, cf. Fig. 1. To enable EH and information transmission in the uplink at the user devices, we adopt time-division-duplex (TDD) transmission and assume that each time frame of length T_{f} is divided into two subframes. In particular, in the first subframe of length $\bar{\tau}T_{\text{f}}$ with $\bar{\tau} \in [0, 1]$, the BS transmits an RF energy signal to transfer energy to the user devices, which harvest the received power. In the subsequent subframe of length $(1-\bar{\tau})T_{\text{f}}$, this harvested power is utilized for information transmission

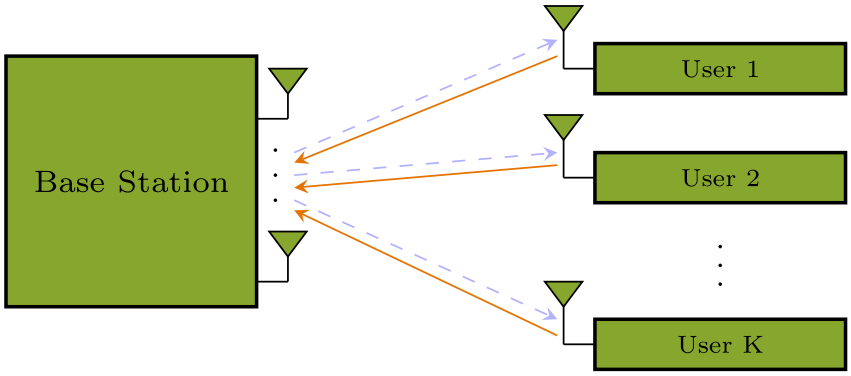

Fig. 1. A WPCN with a multi-antenna BS and K single-antenna users. In the downlink, the BS sends an energy signal to the users (blue dashed arrows). In turn, the users harvest the received energy and utilize it for information transmission in the uplink (orange solid arrows).

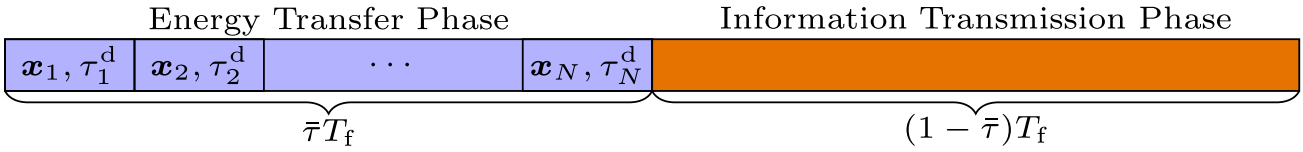

Fig. 2. Structure of a time frame of length T_{f}.

in the uplink. We assume block fading channels between the BS and user devices, i.e., the channel of user $k, k \in \{1, 2, \cdots, K\}$, is constant for the duration of a time frame but may change independently from one time frame to the next. The channel between the BS and user k is characterized by row vector[1] $\boldsymbol{h}_k \in \mathbb{C}^{1\times N_{\mathrm{t}}}$. Furthermore, to investigate the maximum achievable performance of WPCNs, as in, e.g., [22], [23], [25], and [24], we assume that channel reciprocity holds and $\boldsymbol{h}_k$ is perfectly known[2] at the BS.

A. Energy Transfer Phase

In the energy transfer phase, in contrast to the WPCN designs in [6], [7], [8], [9], [10], [14], [15], [16], [17], [18], [19], [20], [22], and [23], to jointly optimize transmit beamforming at the BS and waveform of the energy signal, we assume that the BS transmits a pulse-modulated RF energy signal employing a sequence of N energy signal vectors $\boldsymbol{x}_n \in \mathbb{C}^{N_{\mathrm{t}}}$, cf. Fig. 2. The equivalent complex baseband (ECB) representation of this pulse-modulated RF energy signal is modelled as $\boldsymbol{x}(t) = \sum_{n=1}^{N} \boldsymbol{x}_n \psi_n(t) \in \mathbb{C}^{N_{\mathrm{t}}}$, where $\psi_n(t) = \Pi\big(\frac{t-\sum_{k=0}^{n-1} \tau_k^{\mathrm{d}} T_{\mathrm{f}}}{\tau_n^{\mathrm{d}} T_{\mathrm{f}}}\big)$ is the transmit pulse, $\tau_0^{\mathrm{d}} = 0$, $\Pi(t)$ is a rectangular function that takes value 1 if $t \in [0, 1)$ and 0, otherwise. Here, $\tau_n^{\mathrm{d}}, n \in \{1, 2, \cdots, N\}$, is the portion of the time frame of length T_{f} utilized for transmission of energy signal vector $\boldsymbol{x}_n$ with $\sum_{n=1}^{N} \tau_n^{\mathrm{d}} = \bar{\tau}$.[3]

The RF energy signal received at user k in the energy transfer phase is given by

$$z_k^{\mathrm{RF}}(t) = \sqrt{2}\Re\Big\{\boldsymbol{h}_k \boldsymbol{x}(t) \exp(j2\pi f_c t)\Big\}, \tag{1}$$

where f_c denotes the carrier frequency. Similar to [25], we neglect the noise received at the user terminals since its contribution to the harvested power is negligible.

To harvest power, users are equipped with memoryless non-linear EH circuits [1], [24], [25]. In contrast to the WPCN designs in [6], [7], [8], [9], [10], [14], [15], [16], [17], [18], and [19], in this work, we characterize the instantaneous behaviour of an EH circuit and model it via the relationship between the instantaneous received and harvested powers. Furthermore, to take all non-linear and saturation effects of EH circuits into account, we assume that the mapping between the instantaneous received and harvested powers at user k is characterized by a circuit-based function $\phi_k(\cdot)$, which is given by

$$\phi_k(|z|^2) = \min\{\varphi_k(|z|^2), \varphi_k(A_k^2)\}. \tag{2}$$

Here, z is the ECB representation of the received RF energy signal at the user device, $\varphi_k(\cdot), k \in \{1, 2, \cdots, K\}$, is a convex monotonically increasing continuously differentiable function, whose parameters are independent of the received signal and determined by the EH circuit, and A_k is the minimum amplitude of the received signal that drives the EH circuit of user k into saturation [24], [25]. We note that $\varphi_k(\cdot)$ belongs to a wide class of functions, which encompasses models for practical EH circuits, and can be, e.g., linear [6], [7], [8], [9], [10] or derived for a given rectifier circuit as in [13], [20], and [25]. For our

[1]The statistics of channel vectors $\boldsymbol{h}_k, k \in \{1, 2, \cdots, K\}$, may be modelled as, e.g., Rayleigh, Rician, or Nakagami-m fading [8], [10], or via a ray-based model, such as QuaDRiGa [26].

[2]To analyze the performance of WPCNs with imperfect channel knowledge, one can adopt a practical channel estimation scheme at the BS, where a short channel acquisition time slot is added at the beginning of each time frame. In this time slot, the user devices utilize a portion of the energy harvested in the previous time frames for uplink transmission of pilot sequences, which are then exploited at the BS for channel estimation [27]. Furthermore, one can design energy signals and resource allocation schemes for WPCNs which are robust to imperfect channel knowledge [10], [15], [19]. The design of such robust WPCNs is an interesting direction for further research and is beyond the scope of this paper.

[3]We note that with the proposed energy signal model, arbitrary baseband signal waveforms (e.g., sinusoidal waveforms) can be approximated with any desired accuracy as $N \to \infty$ by properly adjusting the downlink transmit symbol vectors $\boldsymbol{x}_n, n \in \{1, 2, \cdots, N\}$. However, in Section III-C, we show that for the optimal energy signal design, the number of downlink transmit symbol vectors N is upper-bounded.

simulation results, we utilize a circuit-based EH model, whose parameters are summarized in Table I introduced in Section V.

Thus, the average power harvested by user k during the energy transfer phase can be expressed as follows

$$p_k^{\mathrm{d}} = \sum_{n=1}^{N} \tau_n^{\mathrm{d}} \phi_k\big(|z_{k,n}|^2\big), \tag{3}$$

where $z_{k,n} = \boldsymbol{h}_k \boldsymbol{x}_n$ is the ECB representative of RF energy signal $z_k^{\mathrm{RF}}(t)$ received in time slot n at user k. Furthermore, we assume that user k is equipped with a rechargeable built-in battery, whose initial energy, q_k, is known[4] at the BS [10].

Thus, at the end of the downlink transmission phase, the amount of energy available at user k is given by

$$e_k(\boldsymbol{X}, \boldsymbol{\tau}^{\mathrm{d}}, N) = q_k + T_{\mathrm{f}} \sum_{n=1}^{N} \tau_n^{\mathrm{d}} \phi_k\big(|\boldsymbol{h}_k \boldsymbol{x}_n|^2\big), \tag{4}$$

where matrix $\boldsymbol{X} = [\boldsymbol{x}_1 \ \boldsymbol{x}_2 \ \cdots \ \boldsymbol{x}_N]$ contains the transmit energy signal vectors and $\boldsymbol{\tau}^{\mathrm{d}} = [\tau_1^{\mathrm{d}}, \tau_2^{\mathrm{d}}, \cdots, \tau_N^{\mathrm{d}}]^\top$ is the vector of time durations allocated to the corresponding time slots.

B. Information Transmission Phase

In the uplink phase, the users transmit information to the BS exploiting the energy available in their batteries. The symbol vector $\boldsymbol{r} \in \mathbb{C}^{N_{\mathrm{t}}}$ received at the BS in the scheduled time slot is given by

$$\boldsymbol{r} = \sum_{k=1}^{K} \boldsymbol{h}_k^H \sqrt{p_k^{\mathrm{u}}} s_k + \boldsymbol{n}, \tag{5}$$

where p_k^{u} is the power utilized by user k for transmission of information symbol $s_k \in \mathbb{C}$, which is modelled as a complex zero-mean and unit-variance Gaussian random variable, and $\boldsymbol{n} \in \mathbb{C}^{N_{\mathrm{t}}}$ is an additive white Gaussian noise (AWGN) vector with zero mean and covariance matrix $\sigma^2 \boldsymbol{I}_{N_{\mathrm{t}}}$. To reduce computational complexity and suppress inter-user interference, we assume ZF equalization[5] at the BS. Thus, the detected information symbol $\hat{s}_k$ of user k at the BS can be expressed as follows:

$$\hat{s}_k = \boldsymbol{f}_k \boldsymbol{r} = \sqrt{p_k^{\mathrm{u}}} s_k + \tilde{n}_k, \tag{6}$$

where $\tilde{n}_k = \boldsymbol{f}_k \boldsymbol{n}$ is the equivalent AWGN with variance $\tilde{\sigma}_k^2 = \|\boldsymbol{f}_k\|_2^2 \sigma^2$ impairing the detected information signal transmitted by user k. Here, equalization vector $\boldsymbol{f}_k \in \mathbb{C}^{1 \times N_{\mathrm{t}}}$ is the k^{th} row of matrix $\boldsymbol{F} = (\boldsymbol{H}_{\mathrm{u}}^H \boldsymbol{H}_{\mathrm{u}})^{-1} \boldsymbol{H}_{\mathrm{u}}^H$, where $\boldsymbol{H}_{\mathrm{u}} = [\boldsymbol{h}_1^H \ \boldsymbol{h}_2^H \ \cdots \ \boldsymbol{h}_K^H]$ is the composite uplink channel between the users and the BS. Finally, the data rate of user k is given by $R_k(\bar{\tau}, p_k^{\mathrm{u}}) = (1-\bar{\tau}) \log_2(1+\Gamma_k)$, where $\Gamma_k = p_k^{\mathrm{u}} / \tilde{\sigma}_k^2$ is the SNR at the BS for the detected information symbol transmitted by user k.

[4]We note that if the initial energies of the user devices are not known at the BS, we can assume $q_k = 0\,\mathrm{J}, \forall k$.

[5]We note that space division multiple access (SDMA) is able to significantly outperform time division multiple access (TDMA) for multi-user information transmission [28]. Furthermore, ZF equalization is close to optimal if a large number of antennas is deployed at the BS, i.e., $N_{\mathrm{t}} \gg K$, which is a preferred regime for wireless power transfer systems, where a significant downlink beamforming gain is generally required to be able to harvest meaningful amounts of power [8], [29].

III. Problem Formulation and Optimal Solution

In this section, in contrast to the WPCN designs in [6], [7], [8], [9], [10], [15], [16], [17], [18], [19], [22], and [23], we develop a framework for the joint optimization of the downlink energy signal waveform and time allocation policy for the adopted general circuit-based EH model in (2). To this end, we first formulate an optimization problem, and then, we determine the optimal solution for single-user and multi-user WPCNs, respectively.

A. Problem Formulation

In the following, we formulate an optimization problem for the minimization of the average transmit power at the BS under per-user rate constraints in the uplink. For a given time frame, the optimal transmit energy signal vectors and time allocation policy are obtained as the solution of the following non-convex optimization problem:

$$\underset{\boldsymbol{\tau}^{\mathrm{d}} \succeq \boldsymbol{0}, \bar{\tau} \in [0,1], \boldsymbol{X}, \boldsymbol{p}^{\mathrm{u}}, N}{\text{minimize}} \quad P_{\mathrm{DL}}(\boldsymbol{\tau}^{\mathrm{d}}, \boldsymbol{X}, N) \tag{7a}$$

$$\text{subject to} \quad R_k(\bar{\tau}, p_k^{\mathrm{u}}) \geq R_k^{\mathrm{req}}, \ \forall k, \tag{7b}$$

$$e_k(\boldsymbol{X}, \boldsymbol{\tau}^{\mathrm{d}}, N) \geq (1-\bar{\tau}) p_k^{\mathrm{u}} T_{\mathrm{f}} + p_k^{\mathrm{req}} T_{\mathrm{f}}, \ \forall k, \tag{7c}$$

$$\sum_{n=1}^{N} \tau^{\mathrm{d}_n} = \bar{\tau}, \tag{7d}$$

where $P_{\mathrm{DL}}(\boldsymbol{\tau}^{\mathrm{d}}, \boldsymbol{X}, N) = \sum_{n=1}^{N} \tau_n^{\mathrm{d}} \|\boldsymbol{x}_n\|_2^2$ and $\boldsymbol{p}^{\mathrm{u}} = [p_1^{\mathrm{u}} \ p_2^{\mathrm{u}} \ \cdots \ p_K^{\mathrm{u}}]^\top$ are the average transmit power in the energy transfer phase and the vector of powers utilized for information transmission in the uplink, respectively. In problem (7), we minimize the average transmit power at the BS (7a) in the energy transfer phase subject to per-user information rate constraints (7b), where R_k^{req} is the required rate of user k in the uplink. Constraint (7c) ensures that the available energy at user k at the end of the energy transfer phase is not lower than the sum of energies that are needed for the uplink information transmission and performing other operational tasks, e.g., sensing, channel estimation, transmission of pilot sequences, and signal processing tasks. Finally, constraint (7d) ensures that the obtained time allocation is feasible, i.e., the normalized portions of the time frame $\tau_n^{\mathrm{d}}, n \in \{1, 2, \cdots, N\}$, utilized for transmission of the downlink energy signal vectors sum up to the total normalized duration of the energy transfer phase $\bar{\tau}$. We assume that the values of R_k^{req} and p_k^{req} are set by user k and communicated to the BS beforehand. We note that in contrast to [6], [7], [8], [9], [10], [14], [15], [16], [17], [18], and [19], where the covariance matrix $\tilde{\boldsymbol{X}} = \sum_{n=1}^{N} \frac{\tau_n^{\mathrm{d}}}{T_{\mathrm{f}}} \boldsymbol{x}_n \boldsymbol{x}_n^H$ of the downlink energy signal is optimized, the circuit-based EH model in (2) allows the direct optimization of the individual transmit energy signal vectors $\boldsymbol{x}_1, \boldsymbol{x}_2, \cdots, \boldsymbol{x}_N$ and their number N or, equivalently, the waveform of signal $\boldsymbol{x}(t)$.

Due to the non-convexity of the objective function (7a) and constraints (7b) and (7c), optimization problem (7) is, in general, difficult to solve. In the following, we first show that for single-user WPCNs, optimization problem (7) can be solved in closed-form. Next, for multi-user WPCNs, we characterize the optimal solution of (7) for the general case and determine it based on a K-dimensional grid search.

B. Single-User WPCNs

In this section, we solve optimization problem (7) for single-user WPCNs and thus, for notational convenience, we drop the subscripts for user 1. The optimal power $p^{\mathrm{u}*}$ for uplink information transmission has to satisfy constraints (7b) and (7c) and thus, can be chosen arbitrarily[6] in the interval $[p^{\mathrm{u}}_{\min}, p^{\mathrm{u}}_{\max}]$. Here, $p^{\mathrm{u}}_{\min} = (2^{\frac{R^{\mathrm{req}}}{1-\bar{\tau}}} - 1)\tilde{\sigma}^2$ is the minimum power required for uplink transmission with required rate R^{req} and $p^{\mathrm{u}}_{\max} = \frac{1}{1-\bar{\tau}}\big(\frac{q}{T_{\mathrm{f}}} - p^{\mathrm{req}} + \sum_n \tau^{\mathrm{d}}_n \phi(|\boldsymbol{h}\boldsymbol{x}_n|^2)\big)$ is the power available at the user device at the end of the energy transfer phase. The optimal time sharing parameter $\bar{\tau}^*$, the normalized lengths of the time slots $\tau^{\mathrm{d}*}_n$, and the transmit energy signal vectors in the downlink $\boldsymbol{x}^*_n, n \in \{1, 2, \cdots, N\}$, can be obtained as the solution of the following optimization problem:

$$\underset{\boldsymbol{\tau}^{\mathrm{d}} \succeq \boldsymbol{0}, \bar{\tau} \in [0,1], \boldsymbol{X}, N}{\text{minimize}} \quad \sum_{n=1}^{N} \tau^{\mathrm{d}}_n \|\boldsymbol{x}_n\|_2^2 \tag{8a}$$

$$\text{subject to} \quad \sum_{n=1}^{N} \tau^{\mathrm{d}}_n \phi(|\boldsymbol{h}\boldsymbol{x}_n|^2) \geq \xi(\bar{\tau}), \tag{8b}$$

$$\sum_{n=1}^{N} \tau^{\mathrm{d}}_n = \bar{\tau}, \tag{8c}$$

where $\xi(\bar{\tau}) = p^{\mathrm{req}} - \frac{q}{T_{\mathrm{f}}} + (1-\bar{\tau})\big(2^{\frac{R^{\mathrm{req}}}{1-\bar{\tau}}} - 1\big)\tilde{\sigma}^2$. We note that similar to (7), problem (8) is still non-convex. However, in the following proposition, we show that the optimal solution of (8) requires only a single energy signal vector, i.e., $N^* = 1$, which is collinear with the MRT vector.

Proposition 1: The optimal transmit signal in the energy transfer phase as solution of problem (8) employs a single energy signal vector $\boldsymbol{x}^* = \boldsymbol{w}^* s^*$, where $\boldsymbol{w}^* = \frac{\boldsymbol{h}^H}{\|\boldsymbol{h}\|_2}$ is the MRT beamformer and $s^* = \alpha^*_s \exp(j\theta_s)$ is a scalar symbol. The magnitude of optimal symbol s^* is given by $\alpha^*_s = \frac{A}{\|\boldsymbol{h}\|_2}$, whereas the phase of s^* can be arbitrarily chosen, i.e., $\theta_s \in [0, 2\pi)$.

Proof: Please refer to Appendix A. ∎

Proposition 1 implies that in the downlink energy transfer phase, the optimal signal consists of a single transmit energy signal vector $\boldsymbol{x}^*$, which is collinear with the MRT beamformer and whose magnitude is chosen to drive the EH circuit into saturation. Exploiting Proposition 1, we determine the optimal $\bar{\tau}^*$ that solves (8) as follows:

$$\bar{\tau}^* = \min\{\bar{\tau} : f_{\mathrm{SU}}(\bar{\tau}) \geq 0\}, \tag{9}$$

where $f_{\mathrm{SU}}(\bar{\tau}) = \bar{\tau}\phi(A^2) - \xi(\bar{\tau})$. Furthermore, if problem (8) is feasible and does not have a trivial solution, i.e., $\bar{\tau}^* \in (0, 1]$, the optimal $\bar{\tau}^*$ can be obtained as the minimum root of equation $f_{\mathrm{SU}}(\bar{\tau}) = 0$, i.e., $\bar{\tau}^* = \min\{\bar{\tau} : f_{\mathrm{SU}}(\bar{\tau}) = 0\}$.

C. Multi-User WPCNs

In this section, we determine the optimal solution of (7) for multi-user WPCNs, i.e., for $K > 1$. First, we reformulate constraint (7b) equivalently as $p^{\mathrm{u}}_k \geq \xi^{\mathrm{u}}_k(\bar{\tau}), \forall k$, where $\xi^{\mathrm{u}}_k(\bar{\tau}) = \tilde{\sigma}^2_k\big(2^{\frac{R^{\mathrm{req}}_k}{1-\bar{\tau}}} - 1\big)$ is the minimum power required by user k for information transmission with rate R^{req}_k. Next, similarly to single-user WPCNs in Section III-B, for given $\bar{\tau}$, $\boldsymbol{\tau}^{\mathrm{d}}$, $\boldsymbol{X}$, and N, the optimal uplink transmit power $p^{\mathrm{u}*}_k$ for user k satisfying constraints (7b) and (7c) can be arbitrarily chosen from the interval $[\xi^{\mathrm{u}}_k(\bar{\tau}), p^{\mathrm{u}}_{\max,k}]$, where $p^{\mathrm{u}}_{\max,k}$ is the maximum power available at user k for uplink transmission and is given by

$$p^{\mathrm{u}}_{\max,k} = \frac{1}{1-\bar{\tau}}\Big(\frac{q_k}{T_{\mathrm{f}}} - p^{\mathrm{req}}_k + \sum_{n=1}^{N} \tau^{\mathrm{d}}_n \phi_k(|\boldsymbol{h}_k\boldsymbol{x}_n|^2)\Big). \tag{10}$$

Then, problem (7) can be simplified as follows:

$$\underset{\boldsymbol{\tau}^{\mathrm{d}} \succeq \boldsymbol{0}, \bar{\tau} \in [0,1], \boldsymbol{X}, N}{\text{minimize}} \quad \sum_{n=1}^{N} \tau^{\mathrm{d}}_n \|\boldsymbol{x}_n\|_2^2 \tag{11a}$$

$$\text{subject to} \quad \sum_{n=1}^{N} \tau^{\mathrm{d}}_n = \bar{\tau}, \tag{11b}$$

$$\sum_{n=1}^{N} \tau^{\mathrm{d}}_n \phi_k\big(|\boldsymbol{h}_k\boldsymbol{x}_n|^2\big) \geq \xi^{\mathrm{d}}_k(\bar{\tau}), \forall k, \tag{11c}$$

where $\xi^{\mathrm{d}}_k(\bar{\tau}) = (1-\bar{\tau})\xi^{\mathrm{u}}_k(\bar{\tau}) + p^{\mathrm{req}}_k - \frac{q_k}{T_{\mathrm{f}}}$ is the required harvested power at user k.

In the following proposition, we characterize the optimal solution of (11).

Proposition 2: The optimal transmit energy signal vectors $\boldsymbol{x}^*_n, n \in \{1, 2, \cdots, N\}$, as solution of (11) can be expressed as follows

$$\boldsymbol{x}^*_n = \boldsymbol{w}^*_n s_n, \tag{12}$$

where $s_n = \exp(j\theta_n), n \in \{1, 2, \cdots, N\}$, are scalar unit-norm symbols with arbitrary phases $\theta_n = [0, 2\pi)$. Energy beamforming vectors $\boldsymbol{w}^*_n$, $n \in \{1, 2, \cdots, N\}$, can be obtained as solutions of the following optimization problem:

$$\underset{\boldsymbol{w}_n}{\text{minimize}} \quad \|\boldsymbol{w}_n\|_2^2 \tag{13a}$$

$$\text{subject to} \quad \phi_k(|\boldsymbol{h}_k\boldsymbol{w}_n|^2) \geq \mu_{n,k}, \forall k. \tag{13b}$$

For each $n \in \{1, 2, \cdots, N\}$, vector $\boldsymbol{\mu}_n = [\mu_{n,1}, \mu_{n,2}, \cdots, \mu_{n,K}]^\top \in \mathbb{R}^K_+$ contains the instantaneous powers harvested at user devices $1, 2, \cdots, K$ in time slot n. Furthermore, the optimal $\bar{\tau}^*$, $\boldsymbol{\tau}^{\mathrm{d}*}$, vectors $\boldsymbol{\mu}^*_n, n \in \{1, 2, \cdots, N\}$, and N^* can be determined as solution of the following resource allocation problem:

$$\underset{\boldsymbol{\tau}^{\mathrm{d}} \succeq \boldsymbol{0}, \bar{\tau} \in [0,1], \boldsymbol{\mu}_1, \cdots, \boldsymbol{\mu}_N, N}{\text{minimize}} \quad \sum_{n=1}^{N} \tau^{\mathrm{d}}_n \psi(\boldsymbol{\mu}_n) \tag{14a}$$

$$\text{subject to} \quad \sum_{n=1}^{N} \tau^{\mathrm{d}}_n \boldsymbol{\mu}_n \succeq \boldsymbol{\xi}^{\mathrm{d}}(\bar{\tau}), \tag{14b}$$

$$\sum_{n=1}^{N} \tau^{\mathrm{d}}_n = \bar{\tau}, \tag{14c}$$

with $\boldsymbol{\xi}^{\mathrm{d}}(\bar{\tau}) = [\xi^{\mathrm{d}}_1(\bar{\tau}), \ \xi^{\mathrm{d}}_2(\bar{\tau}), \ \cdots, \ \xi^{\mathrm{d}}_K(\bar{\tau})]^\top$. Here, $\psi(\boldsymbol{\mu}) : \mathcal{R}^K \to \mathcal{R}$ is a monotonic non-decreasing function given by

$$\psi(\boldsymbol{\mu}) = \min_{\boldsymbol{x} \in \Omega(\boldsymbol{\mu})} \|\boldsymbol{x}\|_2^2 \tag{15}$$

with $\Omega(\boldsymbol{\mu}) = \{\boldsymbol{x} : \phi_k(|\boldsymbol{h}_k\boldsymbol{x}|^2) \geq \mu_k, \forall k\}$.

Proof: Please refer to Appendix B. ∎

[6] We note that for power-efficient communication, if $p^{\mathrm{u}}_{\max} > p^{\mathrm{u}}_{\min}$, the user devices may select $p^{\mathrm{u}*} = p^{\mathrm{u}}_{\min}$ to save power for future use.

Proposition 2 reveals that problem (11) can be solved by first determining function $\psi(\boldsymbol{\mu})$ in (15), and subsequently obtaining the optimal time sharing parameter, number of time slots, their normalized lengths, and vectors of harvested powers[7] in the downlink, $\bar{\tau}^*, N^*, \boldsymbol{\tau}^{\mathrm{d}*}$, and $\boldsymbol{\mu}_n^*, n \in \{1, 2, \cdots, N^*\}$, respectively, as solution of optimization problem (14). Finally, the optimal downlink transmit energy signal vectors in (12) comprise energy beamformers $\boldsymbol{w}_n^*$ and scalar unit-norm symbols[8] s_n. The optimal energy beamforming vectors $\boldsymbol{w}_n^*$ in (12) can be obtained as solutions of the non-convex problem (13).

In the following, we separately solve optimization problems (13), (14), and (15). Although problems (13) - (15) are non-convex, we show that the computational complexity of solving (14) and (15) depends on the number of users K and is independent of the number of BS antennas N_{t}, whereas the solution of (13) has a computational complexity that is polynomial in N_{t}.

1) Solution of Problem (15): In this section, for any given vector $\boldsymbol{\mu} \in \mathcal{R}^K$, we determine the value of function $\psi(\boldsymbol{\mu})$ in (15). To this end, in the following proposition, we show that problem (15) can be equivalently reformulated as a convex optimization problem.

Proposition 3: For a given vector $\boldsymbol{\mu} \in \mathcal{R}^K$, the value of function $\psi(\boldsymbol{\mu})$ can be determined as solution of the following convex optimization problem:

$$\psi(\boldsymbol{\mu}) = \max_{\boldsymbol{\lambda} \succeq \mathbf{0}} \ \boldsymbol{\rho}^\top \boldsymbol{\lambda} \quad \text{subject to } \|\boldsymbol{B}\,\mathrm{diag}(\boldsymbol{\lambda})\boldsymbol{B}\|_2 \leq 1, \tag{16}$$

where $\boldsymbol{\lambda} \in \mathbb{R}^K$, $\rho_k = \phi_k^{-1}(\mu_k), k \in \{1, 2, \cdots, K\}$, and $\boldsymbol{B} = (\boldsymbol{H}\boldsymbol{H}^H)^{\frac{1}{2}}$ with $\boldsymbol{H} = \boldsymbol{H}_u^H = [\boldsymbol{h}_1^H\ \boldsymbol{h}_2^H\ \cdots\ \boldsymbol{h}_K^H]^H$.

Proof: Please refer to Appendix C. ■

Proposition 3 reveals that, for any given $\boldsymbol{\mu}$, the value of $\psi(\boldsymbol{\mu})$ can be obtained as a solution of the convex optimization problem (16) via a standard numerical optimization tool, such as CVX [31]. Furthermore, we highlight that the computational complexity of (16) does not depend on the number of transmit antennas N_{t} [32].

2) Solution of Problem (14): In the following, for function $\psi(\boldsymbol{\mu})$ introduced in (15), we solve optimization problem (14). To this end, in the following proposition, we first show that for any function $\psi(\boldsymbol{\mu})$, the optimal value of N satisfies $N^* \leq K+1$. Next, we propose a grid search algorithm to solve (14).

Proposition 4: For any given function $\psi(\boldsymbol{\mu})$, the optimal number of time slots for the downlink power transfer phase satisfies $N^* \leq K+1$.

Proof: Please refer to Appendix D. ■

Proposition 4 provides an upper bound on the optimal number of time slots N^* in the downlink phase. Therefore, to find the optimal solution of (14), we set $N = \bar{N} = K+1$ and determine the optimal $\bar{\tau}^* \in [0,1]$, $\boldsymbol{\tau}^{\mathrm{d}*} \in [0,1]^{\bar{N}}$, and $\boldsymbol{\mu}_n^*, n \in \{1, 2, \cdots, \bar{N}\}$, as solution of the resulting optimization problem.

In the following, we exploit a grid search to solve (14). First, we define a uniform grid $\mathcal{P}_\tau = \{\bar{\tau}_1, \bar{\tau}_2, \cdots \bar{\tau}_{L_\tau}\}$ of size L_τ, where $\bar{\tau}_p = \frac{p-1}{L_\tau - 1}, p \in \{1, 2, \cdots L_\tau - 1\}$. Next, we obtain the optimal $\boldsymbol{\tau}^{\mathrm{d}*}$ and $\boldsymbol{\mu}_n^*, n \in \{1, 2, \cdots, \bar{N}\}$, for each $\bar{\tau} \in \mathcal{P}_\tau$, i.e., we solve the following optimization problem:

$$\underset{\boldsymbol{\tau}^{\mathrm{d}} \succeq \mathbf{0}, \boldsymbol{\mu}_1, \cdots, \boldsymbol{\mu}_{\bar{N}}}{\text{minimize}} \quad \sum_{n=1}^{\bar{N}} \tau_n^{\mathrm{d}} \psi(\boldsymbol{\mu}_n) \tag{17a}$$

$$\text{subject to} \quad \sum_{n=1}^{\bar{N}} \tau_n^{\mathrm{d}} \mu_{n,k} \geq \xi_k^{\mathrm{d}}(\bar{\tau}), \tag{17b}$$

$$\sum_{n=1}^{\bar{N}} \tau_n^{\mathrm{d}} = \bar{\tau}. \tag{17c}$$

To this end, we first define the uniform grids $\mathcal{P}_k = \{\hat{\mu}_{1,k}, \hat{\mu}_{2,k}, \cdots, \hat{\mu}_{L_\mu,k}\}, k \in \{1, 2, \cdots, K\}$, of size L_μ that span the feasible intervals of harvested powers at users $k, k \in \{1, 2, \cdots, K\}$. We note that the harvested powers $\mu_{n,k}, n \in \{1, 2, \cdots, \bar{N}\}, k \in \{1, 2, \cdots, K\}$, are bounded, i.e., $\mu_{n,k} \in [0, \varphi_k(A_k^2)], \forall n, k$. Thus, the elements of grid $\mathcal{P}_k$ are given by $\hat{\mu}_{j,k} = \frac{(j-1)\varphi_k(A_k^2)}{L_\mu - 1}$, $j \in \{1, 2, \cdots, L_\mu\}$, $k \in \{1, 2, \cdots, K\}$. Next, based on grids $\mathcal{P}_k, k \in \{1, 2, \cdots, K\}$, we construct another grid $\mathcal{P}_\mu$ of size L_μ^K, whose elements are vectors $\bar{\boldsymbol{\mu}}_j = [\bar{\mu}_{j,1}, \bar{\mu}_{j,2}, \cdots, \bar{\mu}_{j,K}]^\top$, $j \in \{1, 2, \cdots, L_\mu^K\}$, representing unique combinations of harvested powers at the user devices, i.e., for any $i \neq j$, we have $\bar{\boldsymbol{\mu}}_i \neq \bar{\boldsymbol{\mu}}_j$. To uniquely define vector $\bar{\boldsymbol{\mu}}_j$, we consider the representation of $j-1$ in the numeral system with base L_μ, $j \in \{1, 2, \cdots L_\mu^K\}, k \in \{1, 2, \cdots, K\}$, i.e., $i_k \in \{0, 1, \cdots, L_\mu - 1\}$ and $j = \sum_{k=1}^K i_k L_\mu^{K-k} + 1$, and set the elements of $\bar{\boldsymbol{\mu}}_j$ to values $\bar{\mu}_{j,k} = \frac{i_k \phi_k(A_k^2)}{L_\mu - 1}$, where i_k is the digit in position k in the representation of $j-1$.

Finally, we solve (17) on the grid $\mathcal{P}_\mu$, i.e., we optimally select the $K+1$ elements of $\mathcal{P}_\mu$ with non-zero[9] normalized time durations. To this end, we solve the following linear optimization problem:

$$\underset{\tilde{\boldsymbol{\tau}}^{\mathrm{d}} \succeq \mathbf{0}}{\text{minimize}} \quad \sum_{j=1}^{L_\mu^K} \tilde{\tau}_j^{\mathrm{d}} \psi(\bar{\boldsymbol{\mu}}_j) \tag{18a}$$

$$\text{subject to} \quad \boldsymbol{M}\tilde{\boldsymbol{\tau}}^{\mathrm{d}} \succeq \boldsymbol{\xi}^{\mathrm{d}}(\bar{\tau}), \tag{18b}$$

$$\sum_{j=1}^{L_\mu^K} \tilde{\tau}_j^{\mathrm{d}} = \bar{\tau}, \tag{18c}$$

where $\boldsymbol{M} = [\bar{\boldsymbol{\mu}}_1, \bar{\boldsymbol{\mu}}_2, \cdots, \bar{\boldsymbol{\mu}}_{L_\mu^K}] \in \mathbb{R}^{K \times L_\mu^K}$ and $\tilde{\boldsymbol{\tau}}^{\mathrm{d}} \in [0,1]^{L_\mu^K}$. Since problem (18) is linear, it can be efficiently solved using a standard numerical optimization tool, such as CVX [31]. Finally, we choose the $\bar{\tau}^* \in \mathcal{P}_\tau$ that yields the minimum transmit power in the downlink. For the optimal $\bar{\tau}^*$, the optimal normalized lengths of the time slots $\boldsymbol{\tau}^{\mathrm{d}*}$ and the corresponding vectors of harvested powers $\boldsymbol{\mu}_n^*$, $n \in \{1, 2, \cdots, \bar{N}\}$, are obtained[10] as the $\bar{N}$ non-zero elements of $\tilde{\boldsymbol{\tau}}^{\mathrm{d}*}(\bar{\tau}^*)$ and the

[7] We note that for the optimal solution of optimization problem (7), the EH circuits at the user devices may be driven into an interior point of the saturation region, i.e., we may have $|\boldsymbol{h}_k \boldsymbol{x}_n| > A_k$ for some $n \in \{1, 2, \cdots, N\}$ and $k \in \{1, 2, \cdots, K\}$. This may occur, e.g., if the user devices are collocated and have different required rates R_k^{req} and powers p_k^{req} [30].

[8] Since scalar phase θ_n of s_n^* can be chosen arbitrarily, it can be utilized for, e.g., the transmission of power values $p_k^{\mathrm{u}}, k \in \{1, 2, \cdots, K\}$, and time allocation variables $\boldsymbol{\tau}^{\mathrm{d}}$ and $\bar{\tau}$ to the user devices in the downlink [24].

[9] In our simulations, we observe that for the optimal time allocation $\bar{\tau}^*$, the number of elements of P_μ with non-zero normalized time durations is typically $N^* \leq K$.

Algorithm 1 Algorithm for Determining the Optimal Solution of (14)

Initialize: Grid sizes L_μ and L_τ, channel covariance matrix $\boldsymbol{B} = (\boldsymbol{H}\boldsymbol{H}^H)^{\frac{1}{2}}$, required rate R_k^{req}, required power p_k^{req}, and initial energy q_k at user k for $k \in \{1, 2, \cdots, K\}$.

1. Create grid $\mathcal{P}_\mu$ and calculate $\psi(\cdot)$ on its vertices:

for $j = 0$ to $L_\mu^K - 1$ **do**

1.1. Create vector $\bar{\boldsymbol{\mu}}_j = [\bar{\mu}_{j,1}\ \bar{\mu}_{j,2}\ \cdots\ \bar{\mu}_{j,K}]^\top$, where $\bar{\mu}_{j,k} = \frac{i_k\, \phi_k(A_k^2)}{L_\mu - 1}$, $i_k \in \{0, 1, \cdots, L_\mu\}$, and $j = \sum_{k=1}^{K} i_k L_\mu^{K-k} + 1$

1.2. Calculate $\psi_j = \psi(\bar{\boldsymbol{\mu}}_j)$ as solution of (16)

end

2. Create grid $\mathcal{P}_\tau$ and solve (18) for each point on the grid:

for $p = 1$ to L_τ **do**

2.1. Calculate the time sharing parameter $\bar{\tau}_p = \frac{p-1}{L_\tau - 1}$

2.2. For $\bar{\tau} = \bar{\tau}_p$, determine $\tilde{\boldsymbol{\tau}}_p^{\text{d}*}$ as solution of (18) and the corresponding value $\Psi_p^* = \boldsymbol{\psi}^\top \tilde{\boldsymbol{\tau}}_p^{\text{d}*}$

end

3. Find $p^* = \arg\min_p \Psi_p^*$, the ratio $\bar{\tau}^* = \bar{\tau}_{p^*}$, and the corresponding vectors $\boldsymbol{\tau}^{\text{d}*}$ and $\boldsymbol{\mu}_n^*, n \in \{1, 2, \cdots, \bar{N}\}$

Output: Optimal parameter $\bar{\tau}^*$, time slot lengths $\boldsymbol{\tau}^{\text{d}*}$, and harvested powers $\boldsymbol{\mu}_n^*, n \in \{1, 2, \cdots, \bar{N}\}$

corresponding elements of $\mathcal{P}_\mu$, respectively, where $\tilde{\boldsymbol{\tau}}^{\text{d}*}(\bar{\tau})$ is the solution of (18) for a given $\bar{\tau}$.

The algorithm for determining the optimal solution of problem (14) is summarized in Algorithm 1. We note that the computational complexity of the algorithm is exponential in the number of users K but does not depend on the number of transmit antennas N_{t} employed at the BS.

3) Solution of Problem (13): In the following, for the optimal vectors $\boldsymbol{\mu}_n^*$ obtained in Section III-C.2, we determine the optimal energy beamforming vectors $\boldsymbol{w}_n^*, n \in \{1, 2, \cdots, \bar{N}\}$, as a solution of problem (13). Due to the non-concavity of $\phi_k(\cdot), k \in \{1, 2, \cdots, K\}$, problem (13) is non-convex. Nevertheless, in the following, we show that problem (13) can be equivalently formulated as a convex optimization problem, whose solution has a computational complexity, which is polynomial in N_{t}.

[10]We note that, as the grid size L_μ grows, the optimal solution of (18), i.e., the $\bar{N}$ non-zero elements of vector $\tilde{\boldsymbol{\tau}}^{\text{d}*}(\bar{\tau})$ and the corresponding elements of $\mathcal{P}_\mu$, converges to the optimal solution of (7) for a given $\bar{\tau}$, i.e., $\boldsymbol{\tau}^{\text{d}*}$ and $\boldsymbol{\mu}_n^*, n \in \{1, 2, \cdots, \bar{N}\}$, at the expense of an increase in computational complexity, see (22), [33], [34], [35].

Since problem (13) can be reformulated as a rank-constrained semidefinite optimization problem [24], in the following lemma, we first consider a class of convex semidefinite optimization problems with linear constraints and show that the solutions of such problems are low-rank. The result of this lemma is then exploited for the solution of problem (13).

Lemma 1: For any given vector $\boldsymbol{b} \in \mathbb{R}^K$, the optimal solution of the following convex optimization problem

$$\underset{\boldsymbol{X} \in \mathcal{S}_+^{N_t}}{\text{minimize}} \quad \text{Tr}\{\boldsymbol{X}\} \tag{19a}$$

$$\text{subject to} \quad \boldsymbol{h}_k \boldsymbol{X} \boldsymbol{h}_k^H \geq b_k,\ \forall k \in \{1, 2, \cdots, K\}, \tag{19b}$$

satisfies[11] $\text{rank}\{\boldsymbol{X}\} \leq 1$.

Proof: Please refer to Appendix E. ∎

Next, in the following proposition, we equivalently formulate (13) as a convex optimization problem.

Proposition 5: The optimal energy beamforming vectors $\boldsymbol{w}_n^*, n \in \{1, 2, \cdots, \bar{N}\}$, are given by $\boldsymbol{w}_n^* = \gamma_n \boldsymbol{v}_n$, where γ_n and $\boldsymbol{v}_n$ are the dominant eigenvalue and the corresponding eigenvector of matrix $\boldsymbol{W}_n^*$, which is obtained as solution of the following convex optimization problem:

$$\underset{\boldsymbol{W}_n \in \mathcal{S}_+^{N_t}}{\text{minimize}} \quad \text{Tr}\{\boldsymbol{W}_n\} \tag{20a}$$

$$\text{subject to} \quad \boldsymbol{h}_k \boldsymbol{W}_n \boldsymbol{h}_k^H \geq \varphi_k^{-1}(\mu_{n,k}^*),\ \forall k. \tag{20b}$$

Proof: Since function $\phi_k(\cdot)$ is monotonically non-decreasing, problem (13) can be equivalently reformulated as follows

$$\underset{\boldsymbol{W}_n \in \mathcal{S}_+^{N_t}}{\text{minimize}} \quad \text{Tr}\{\boldsymbol{W}_n\} \tag{21a}$$

$$\text{subject to} \quad \boldsymbol{h}_k \boldsymbol{W}_n \boldsymbol{h}_k^H \geq \varphi_k^{-1}(\mu_{n,k}^*),\ \forall k, \tag{21b}$$

$$\text{rank}\{\boldsymbol{W}_n\} \leq 1. \tag{21c}$$

Problems (20) and (21) are equivalent thanks to Lemma 1. Then, the optimal energy beamforming vector $\boldsymbol{w}_n^*, n \in \{1, 2, \cdots, \bar{N}\}$, as solution of (13) can be determined as $\boldsymbol{w}_n^* = \gamma_n \boldsymbol{v}_n$, where γ_n and $\boldsymbol{v}_n$ are the dominant eigenvalue and the corresponding eigenvector of matrix $\boldsymbol{W}_n^*$, which is the solution of (21). This concludes the proof. ∎

Proposition 5 reveals that the optimal energy beamforming vectors $\boldsymbol{w}_n^*, n \in \{1, 2, \cdots, \bar{N}\}$, can be determined as solution of convex optimization problem (20). We note that (20) can be efficiently solved using numerical optimization tools, such as CVX [31].

Thus, to optimally solve optimization problem (7), we first determine the optimal time allocation $\bar{\tau}^*$, $\boldsymbol{\tau}^{\text{d}*}$, and the optimal vectors of harvested powers $\boldsymbol{\mu}_n^*, n \in \{1, 2, \cdots, \bar{N}\}$, with Algorithm 1. Next, for this optimal time allocation and harvested powers at the user devices, we determine the optimal beamforming vectors $\boldsymbol{w}_n^*, n \in \{1, 2, \cdots, \bar{N}\}$, according to Proposition 5. The algorithm for determining the optimal solution of problem (7) is summarized in Algorithm 2. The

[11]We note that if $b_k = 0, \forall k$, the optimal solution satisfies $\text{rank}\{\boldsymbol{X}\} = 0$. Otherwise, we have $\text{rank}\{\boldsymbol{X}\} = 1$.

Algorithm 2 Optimal Design of Multi-User WPCN.

Initialize: Channel vectors $\boldsymbol{h}_1, \boldsymbol{h}_2, \cdots, \boldsymbol{h}_K$, required rates R_k^{req}, power p_k^{req}, and initial energy q_k at user $k, k \in \{1, 2, \cdots, K\}$.

1. Find the channel covariance matrix $\boldsymbol{B} = (\boldsymbol{H}\boldsymbol{H}^H)^{\frac{1}{2}}$
2. Determine the optimal time allocation $\bar{\tau}^*$, $\boldsymbol{\tau}^{\text{d}*}$, and harvested powers $\boldsymbol{\mu}_n^*, n \in \{1, 2, \cdots, \bar{N}\}$, with Algorithm 1
3. For the optimal harvested powers, determine the energy beamforming vectors $\boldsymbol{w}_n^*$ in Proposition 5

Output: Energy beamforming vectors $\boldsymbol{w}_n^*, n \in \{1, 2, \cdots, \bar{N}\}$, ratio $\bar{\tau}^*$, and time slot lengths $\boldsymbol{\tau}^*$

computational complexity of the optimal WPCN design as function of N_{t} and K is given by

$$\Theta_{\text{Opt}}(N_{\text{t}}, K) = \Theta_{\text{RA}}(N_{\text{t}}, K) + \Theta_{\text{BF}}(N_{\text{t}}, K), \tag{22}$$

where $\Theta_{\text{RA}}(N_{\text{t}}, K) = \mathcal{O}\big(L_\tau L_\mu^K K^3\big)$ and $\Theta_{\text{BF}}(N_{\text{t}}, K) = \mathcal{O}\big(K^2 N_{\text{t}}^{\frac{7}{2}} + K^3 N_{\text{t}}^{\frac{5}{2}} + K^4 N_{\text{t}}^{\frac{1}{2}}\big)$ are the computational complexities of the optimal resource allocation scheme in Algorithm 1 and the optimal energy beamforming design, i.e., the solution of (20), respectively. Here, $\mathcal{O}(\cdot)$ denotes the big-O notation[12]. Thus, we conclude that the computational complexity of the optimal energy signal and resource allocation policy is exponential in the number of deployed users K and polynomial in the number of transmit antennas N_{t}. Hence, determining the optimal WPCN design may not be computationally efficient for multi-user systems with $K \gg 1$. Therefore, in the following section, we propose two suboptimal low-complexity schemes to solve optimization problem (7).

IV. Low-Complexity Design of Multi-User WPCNs

In this section, we propose two suboptimal low-complexity schemes for WPCN design. To this end, we first consider asymptotic massive MISO WPCNs with $N_{\text{t}} \to \infty$ and determine the optimal transmit policy in the downlink in closed-form. Next, based on this result, we propose an MRT-based scheme for WPCN design, which is optimal for massive MISO WPCNs with vanishing system loads and provides a suboptimal solution of (7) for general MISO WPCNs with finite system loads. Finally, to improve the performance of this design for the general case, we derive a low-complexity suboptimal scheme that utilizes SDR.

[12]The computational complexities of a linear program and a convex semidefinite problem that involve n variables and m constraints are given by $\mathcal{O}\big(m^3 + nm^2 + n^2\big)$ and $\mathcal{O}\big(\sqrt{n}(mn^3 + m^2n^2 + m^3)\big)$, respectively [32].

A. Massive MISO WPCNs

In the following, we consider the optimal design of multi-user MISO WPCNs, where the channel vectors $\boldsymbol{h}_k, k \in \{1, 2, \cdots, K\}$, become orthogonal, i.e., $\boldsymbol{h}_i \boldsymbol{h}_j^H = 0, \forall i \neq j$, as the WPCN load approaches zero, i.e., $\frac{K}{N_{\text{t}}} \to 0$ [8]. We note that this property holds for, e.g., massive MISO WPCNs with Rayleigh fading channels as the number of antennas N_{t} at the BS tends to infinity [8], [29].

To solve optimization problem (7), we first determine the optimal fraction $\bar{\tau}^*$ using a one-dimensional grid search as $\bar{\tau}^* = \arg\min_{\bar{\tau} \in [0,1]} P_{\text{DL}}^*(\bar{\tau})$, where

$$P_{\text{DL}}^*(\bar{\tau}) = \min_{\mathcal{F}} \{P_{\text{DL}}\} \tag{23}$$

with $\mathcal{F} = \{\boldsymbol{\mathcal{W}}, \boldsymbol{\tau}^{\text{d}} : \sum_{n=1}^{\bar{N}} \tau_n^{\text{d}} \phi_k\big(|\boldsymbol{h}_k \boldsymbol{w}_n|^2\big) \geq \xi_k^{\text{d}}(\bar{\tau}), \forall k; \sum_{n=1}^{\bar{N}} \tau_n^{\text{d}} = \bar{\tau}\}$, $\boldsymbol{\mathcal{W}} = \{\boldsymbol{w}_1, \boldsymbol{w}_2, \cdots, \boldsymbol{w}_{\bar{N}}\}$, and $P_{\text{DL}} = \sum_{n=1}^{\bar{N}} \tau_n^{\text{d}} \|\boldsymbol{w}_n\|_2^2$.

Next, for a given $\bar{\tau}$, in the following proposition, we show that for massive MISO WPCNs, the optimal energy signal and time allocation policy as solution of (11) can be obtained in closed-form.

Proposition 6: If channel vectors $\boldsymbol{h}_k, k \in \{1, 2, \cdots, K\}$, are orthogonal, i.e., $\boldsymbol{h}_i \boldsymbol{h}_j^H = 0, \forall i \neq j$, for a given $\bar{\tau}$, the K energy beamforming vectors of the optimal energy signal in Proposition 2 and the normalized lengths of the corresponding time slots are given by

$$\boldsymbol{w}_n^* = \sum_{i=n}^{K} A_{k_i} \frac{\boldsymbol{h}_{k_i}^H}{\|\boldsymbol{h}_{k_i}\|_2^2}, \tag{24}$$

$$\tau_n^{\text{d}*} = \bar{t}_{k_n}^+(\bar{\tau}) - \bar{t}_{k_{n-1}}^+(\bar{\tau}), n \in \{1, 2, \cdots, K\}, \tag{25}$$

with $\bar{t}_{k_0}^+(\bar{\tau}) = 0$, respectively. Here, the elements of $\bar{\boldsymbol{t}}^+(\bar{\tau}) = [\bar{t}_{k_1}^+(\bar{\tau}), \bar{t}_{k_2}^+(\bar{\tau}), \cdots, \bar{t}_{k_K}^+(\bar{\tau})] \in \mathbb{R}_+^K$ are obtained by sorting the values $t_k^+(\bar{\tau}) = \max\big\{0, \frac{\xi_k^{\text{d}}(\bar{\tau})}{\phi_k(A_k^2)}\big\}, k \in \{1, 2, \cdots, K\}$, in ascending order. Furthermore, the $(K+1)^{th}$ energy beamforming vector is the all-zero vector, i.e., $\boldsymbol{w}_{K+1}^* = \boldsymbol{0}$, and its normalized length is given by $\tau_{K+1}^{\text{d}*} = \bar{\tau} - \sum_{n=1}^{K} \tau_n^{\text{d}*}$. Finally, the corresponding optimal transmit power in the downlink is given by $P_{\text{DL}}^*(\bar{\tau}) = \sum_{k=1}^{K} \frac{A_k^2}{\|\boldsymbol{h}_k\|_2^2} \frac{\xi_k^{\text{d}}(\bar{\tau})}{\phi_k(A_k^2)}$.

Proof: Please refer to Appendix F. ∎

Proposition 6 reveals that for multi-user massive MISO WPCNs, the optimal energy signal comprises a sequence of weighted sums of MRT beamforming vectors and can be obtained in closed-form. Furthermore, similar to the single-user WPCN in Section III-B, the magnitudes of the MRT beamforming vectors in $\boldsymbol{w}_n^*, n \in \{1, 2, \cdots, \bar{N}\}$, are chosen to drive the corresponding EH circuits at the user devices into saturation. Thus, in the first time slot, it is optimal to drive all EH circuits into saturation. The corresponding normalized time slot duration depends on the power required by the least demanding user k_1, i.e., the user with the minimum normalized required power $\frac{\xi_k^{\text{d}}(\bar{\tau})}{\phi_k(A_k^2)}, k \in \{1, 2, \cdots, K\}$. Furthermore, since the channel vectors $\boldsymbol{h}_k, k \in \{1, 2, \cdots, K\}$, are orthogonal, for the optimal resource allocation policy, in each subsequent time slot, it is optimal to switch-off the power transmission to the user whose power requirement is already satisfied, cf.

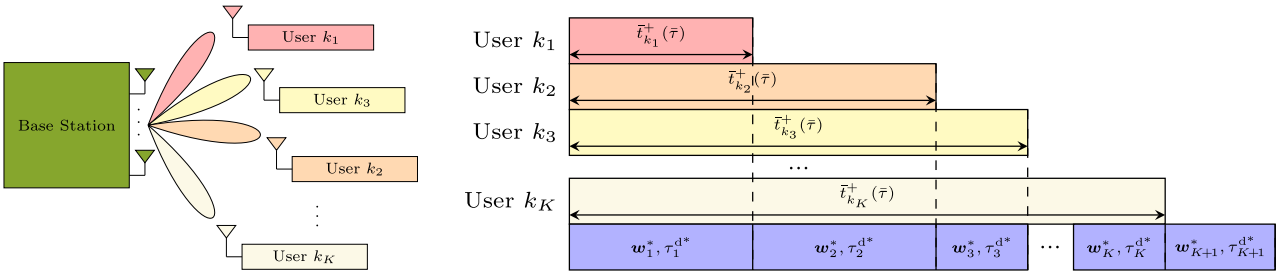

Fig. 3. Optimal design of massive MISO WPCNs. The optimal energy beamforming vectors in the downlink are weighted sums of MRT beamformers, where the weights are chosen such that the corresponding EH circuits are driven into saturation.

Fig. 3. Finally, in the $(K+1)^{\text{th}}$ time slot, all constraints in (11) are satisfied and, hence, the corresponding optimal beamforming vector is the all-zero vector. We note that since the time reserved for the last time slot can be utilized for uplink information transmission, for the optimal $\bar{\tau}^*$, we have $\tau^{\mathrm{d}*}_{K+1} = 0$.

Remark 1: The optimal downlink energy signal for massive MISO systems as solution of problem (7) may not be unique. For example, the order in which $\boldsymbol{w}^*_1, \boldsymbol{w}^*_2, \cdots, \boldsymbol{w}^*_{K+1}$ are transmitted can be chosen arbitrarily. Furthermore, the optimal normalized durations of the time slots may differ from those in Proposition 6 if, e.g., the time slot of user k_1 is split into several parts to serve this user in multiple non-consecutive time slots.

In the following, we exploit Proposition 6 for the derivation of suboptimal WPCN designs. In particular, we first propose a closed-form suboptimal MRT-based WPCN design that is optimal for massive MISO WPCNs with vanishing system loads and is a feasible point of optimization problem (7) for multi-user MISO WPCNs with finite system loads. Next, exploiting SDR, we derive a low-complexity suboptimal scheme that is based on the MRT-based WPCN design and yields a scheme with reduced required average transmit power at the BS in the general case.

B. Suboptimal MRT-Based Scheme

In this section, based on the optimal energy beamforming vectors for massive MISO WPCNs with vanishing system loads in Proposition 6, we propose a suboptimal MRT-based WPCN design that is optimal for massive MISO WPCNs and solves (7) for general multi-user WPCNs. We note that the scheme in Proposition 6 may not be a feasible solution of (7) for the general case since the energy beamforming vectors in Proposition 6 may not be able to drive the corresponding EH circuits into saturation if the channel vectors are not orthogonal. Thus, in the following, we adapt the energy beamforming vectors in Proposition 6 to the case of general WPCNs with finite system loads.

To this end, for a given $\bar{\tau}$, we first determine the energy beamforming vectors $\boldsymbol{w}^*_n$ and the normalized lengths of the corresponding time slots $\tau^{\mathrm{d}*}_n, n \in \{1, 2, \cdots, K+1\}$, as in Proposition 6. Next, to drive the EH circuits of users $k \in \mathcal{K}(n) = \{k_n, k_{n+1}, \cdots, k_K\}$ into saturation, in time slot n, we adopt a weighted energy beamforming vector $\tilde{\boldsymbol{w}}^*_n = \omega_n \boldsymbol{w}^*_n$. We propose to choose the weights $\omega_n, n \in \{1, 2, \cdots, \bar{N}\}$, as follows:

$$\omega_n = \max_{k' \in \mathcal{K}(n)} \frac{A_{k'}}{|\boldsymbol{h}_{k'} \boldsymbol{w}^*_n|}. \tag{26}$$

We note that since $\boldsymbol{w}^*_n$ in Proposition 6 is a weighted sum of random channel vectors $\boldsymbol{h}_{k'}$ of users $k' \in \mathcal{K}(n)$, we have $|\boldsymbol{h}_{k'} \boldsymbol{w}^*_n| > 0$ and $\omega_n < \infty, \forall n$, with probability 1. Furthermore, in the case of orthogonal channel vectors, we have $\omega_n = 1, \forall n \in \{1, 2, \cdots, K\}$, and $\tilde{\boldsymbol{w}}^*_n = \boldsymbol{w}^*_n$. The algorithm proposed to obtain the suboptimal MRT-based WPCN design is summarized in Algorithm 3.

In the proposed suboptimal MRT-based scheme, similar to Proposition 6, energy beamforming vector $\tilde{\boldsymbol{w}}^*_n$ in time slot n, $n \in \{1, 2, \cdots, \bar{N}\}$, is chosen to drive the EH circuits of the users in $\mathcal{K}(n)$ into saturation and, thus, the proposed scheme is a feasible solution of (7). However, this scheme may not be efficient for general multi-user WPCNs with finite system loads since the EH circuits at the user devices may be driven too deep into saturation, i.e., $|\boldsymbol{h}_k \tilde{\boldsymbol{w}}^*_n|^2 > A^2_k$ for some $n \in \{1, 2, \cdots, K\}$ and $k \in \{1, 2, \cdots, \bar{N}\}$, and thus, the constraints in (7b) and (7c) may not be tight. Therefore, to cope with this issue, in the next section, we propose a low-complexity suboptimal scheme that is initialized by the solution attained with the suboptimal MRT-based scheme and yields a scheme with reduced average transmit power in the energy transfer phase for general WPCNs.

C. Suboptimal SDR-Based Scheme

Since the MRT-based WPCN design obtained with Algorithm 3 may be severely suboptimal if the system load $\frac{K}{N_{\mathrm{t}}}$ does not tend to 0, in this section, we improve the performance of the proposed suboptimal design for the general case. In [1], we developed an iterative algorithm that converges to a stationary point of (7). However, since the complexity of this algorithm may be unreasonably high, in this work, we propose a low-complexity solution of (7) that is based on SDR and the MRT-based scheme, which is optimal for massive MISO WPCNs with vanishing system loads.

Since the beamforming vectors $\tilde{\boldsymbol{w}}^*_n, n \in \{1, 2, \cdots, \bar{N}\}$, obtained with Algorithm 3 may drive the EH circuits at the user devices too deep into saturation, i.e., $|\boldsymbol{h}_k \tilde{\boldsymbol{w}}^*_n|^2 \gg A^2_k$ for some $k \in \{1, 2, \cdots, K\}$ and $n \in \{1, 2, \cdots, \bar{N}\}$, we propose to modify energy beamforming vectors $\tilde{\boldsymbol{w}}^*_n$ such that the modified vectors $\hat{\boldsymbol{w}}^*_n, n \in \{1, 2, \cdots, \bar{N}\}$, provide the same harvested powers to the users, but avoid the waste of energy and thus, reduce the average transmit power at the

Algorithm 3 Algorithm for Suboptimal MRT-Based Scheme

Initialize: Required rates R_k^{req}, powers p_k^{req}, initial energies $q_k, \forall k$, grid size L_τ
1. Set initial value $\bar{\tau} = 0$, $i = 1$.
repeat
2. Determine vector $\boldsymbol{t}^+(\bar{\tau})$ as in Proposition 6
3. Find $\boldsymbol{w}_n^*$ and $\tau_n^{\text{d}*}$, $n \in \{1, 2, \cdots, \bar{N}\}$, as in Proposition 6
4. Obtain $\tilde{\boldsymbol{w}}_n = \omega_n \boldsymbol{w}_n^*, n \in \{1, 2, \cdots, \bar{N}\}$, with $\omega_n = \max_{k' \in \mathcal{K}(n)} \frac{A_{k'}}{|\boldsymbol{h}_{k'} \boldsymbol{w}_n^*|}$
5. Save $\tilde{\boldsymbol{w}}_n$ and $\tau_n^{\text{d}*}$ in $\boldsymbol{\mathcal{W}}_i^n$ and $\boldsymbol{\tau}_i^n$, $n \in \{1, 2, \cdots, \bar{N}\}$, respectively
6. Calculate $\eta_i = \sum_{n=1}^{\bar{N}} \tau_n^{\text{d}*} \|\tilde{\boldsymbol{w}}_n^*\|_2^2$
7. Set $\bar{\tau} = \bar{\tau} + \frac{1}{L_\tau - 1}$, $i = i + 1$
until $\bar{\tau} \geq 1$;
8. Find index i^* yielding the minimum value in $\boldsymbol{\eta} = [\eta_1, \eta_2, \cdots, \eta_{i-1}]$
Output: $\tilde{\boldsymbol{w}}_n, \tau_n^{\text{d}*}$ from $\boldsymbol{\mathcal{W}}_{i^*}^n$ and $\boldsymbol{\tau}_{i^*}^n$, $\forall n \in \{1, 2, \cdots, \bar{N}\}$, respectively, and $\bar{\tau}^* = \frac{i^* - 1}{L_\tau - 1}$

BS. To this end, in time slot n, we first determine the harvested powers $\tilde{\mu}_{n,k} = \phi_k(|\boldsymbol{h}_k \tilde{\boldsymbol{w}}_n^*|^2)$ that are achieved at user devices $k \in \{1, 2, \cdots, K\}$ with the suboptimal MRT-based scheme. Next, we determine new energy beamforming vectors $\hat{\boldsymbol{w}}_n^*, n \in \{1, 2, \cdots, \bar{N}\}$, such that $\|\hat{\boldsymbol{w}}_n^*\|_2 \leq \|\tilde{\boldsymbol{w}}_n^*\|_2$ and $\phi_k(|\boldsymbol{h}_k \hat{\boldsymbol{w}}_n^*|^2) \geq \tilde{\mu}_{n,k}, \forall n, k$. To this end, in time slot n, we solve the following optimization problem:

$$\underset{\hat{\boldsymbol{W}}_n \in \mathcal{S}_+^{N_{\text{t}}}}{\text{minimize}} \quad \text{Tr}\{\hat{\boldsymbol{W}}_n\} \tag{27a}$$

$$\text{subject to} \quad \boldsymbol{h}_k \hat{\boldsymbol{W}}_n \boldsymbol{h}_k^H \geq \varphi_k^{-1}(\tilde{\mu}_{n,k}), \ \forall k. \tag{27b}$$

Since (27) is a convex semidefinite optimization problem, it can be solved with a numerical optimization tool, such as CVX [31]. Furthermore, similar to problem (20), the optimal solution $\hat{\boldsymbol{W}}_n^*$ of problem (27) satisfies $\text{rank}\{\hat{\boldsymbol{W}}_n^*\} \leq 1, \forall n \in \{1, 2, \cdots, \bar{N}\}$, cf. Lemma 1. Hence, the beamforming vector in time slot $n, n \in \{1, 2, \cdots, \bar{N}\}$, can be obtained as $\hat{\boldsymbol{w}}_n^* = \hat{\gamma}_n^* \hat{\boldsymbol{v}}_n^*$, where $\hat{\gamma}_n^*$ and $\hat{\boldsymbol{v}}_n^*$ are the dominant eigenvalue and the corresponding eigenvector of matrix $\hat{\boldsymbol{W}}^*$, respectively, see Proposition 5.

The resulting suboptimal SDR-based design is summarized in Algorithm 4. We note that since the suboptimal MRT- and SDR-based designs provide identical harvested powers at the user devices, the solution obtained with Algorithm 4 is also a feasible point of problem (7). Furthermore, since problem (27) is similar to (20), the computational complexity of the suboptimal SDR-based scheme is given by

$$\begin{aligned} \Theta_{\text{SDR}}(N_{\text{t}}, K) &= \Theta_{\text{BF}}(N_{\text{t}}, K) \\ &= \mathcal{O}\big(K^2 N_{\text{t}}^{\frac{7}{2}} + K^3 N_{\text{t}}^{\frac{5}{2}} + K^4 N_{\text{t}}^{\frac{1}{2}}\big). \end{aligned} \tag{28}$$

Thus, the computational complexity of the proposed algorithm is polynomial in the number of users K and the number of transmit antennas N_{t} at the BS. We note that since the time allocation parameter $\bar{\tau}^*$ of the SDR-based scheme in Algorithm 4 is found with the low-complexity MRT-based scheme, the computational complexity of the one-dimensional grid search with respect to $\bar{\tau}$ is neglected in (28).

Algorithm 4 Algorithm for Suboptimal SDR-Based Scheme.

Initialize: Channel vectors $\boldsymbol{h}_1, \boldsymbol{h}_2, \cdots, \boldsymbol{h}_K$, required rates R_k^{req}, powers p_k^{req}, and initial energy q_k at user $k, k \in \{1, 2, \cdots, K\}$.
1. Find $\tilde{\boldsymbol{w}}_n, \tau_n^{\text{d}*}, n \in \{1, 2, \cdots, \bar{N}\}$, and $\bar{\tau}^*$ with Algorithm 3
2. Determine the optimal matrices $\hat{\boldsymbol{W}}_n^*, n \in \{1, 2, \cdots, \bar{N}\}$, as solutions of (27)
3. Obtain $\hat{\boldsymbol{w}}_n^* = \hat{\gamma}_n^* \hat{\boldsymbol{v}}_n^*, \forall n$
Output: $\bar{\tau}^*$, τ_n^{d*}, $\hat{\boldsymbol{w}}_n^*, \forall n$

V. Numerical Results

In this section, we evaluate the performance of the proposed schemes for WPCN design via numerical simulations. First, we discuss the adopted system setup. Next, we study the complexity of the proposed optimal and suboptimal schemes. Finally, we analyze the performances of the proposed schemes and compare them with baseline schemes.

A. Simulation Setup

We assume that the elements of channel vectors $\boldsymbol{h}_k, k \in \{1, 2, \cdots, K\}$, are independent Rayleigh fading. Thus, we model the elements of $\boldsymbol{h}_k, k \in \{1, 2, \cdots, K\}$, as $h_{i,k} = \bar{h}_{i,k} \tilde{h}_{i,k}$, where $\bar{h}_{i,k}$ and $\tilde{h}_{i,k}$ are the large and small scale fading components of the channel, respectively. Furthermore, to account for the path loss, we set the large scale fading component between the BS and user device k to $\bar{h}_{i,k} = \frac{c_l}{4\pi d_k f_c}$, where c_l is the speed of light, $f_c = 868$MHz is the carrier frequency, and d_k is the distance between the BS and user $k \in \{1, 2, \cdots, K\}$. The small-scale fading coefficients $\tilde{h}_{i,k}, \forall i, k$, are modelled as independent and identically distributed (i.i.d.) complex circularly-symmetric Gaussian random variables with zero mean and unit variance. Next, for information transmission in the uplink, we assume a noise variance of $\sigma_k^2 = -120$dBM. Additionally, we assume that all user devices are equipped with identical EH circuits and for the circuit-based EH model $\phi_k(\cdot)$ in (2), we adopt the non-linear function $\varphi_k(|z|^2) = \lambda \Big[\mu^{-1} W_0\Big(\mu \exp(\mu) I_0\Big(\nu \sqrt{2|z|^2}\Big) - 1\Big)^2\Big]$ derived in [25] for a half-wave rectifier with a single diode [12]. Here, λ, μ, and ν are parameters that depend on the circuit elements but not on the received signal, whereas $W_0(\cdot)$ and $I_0(\cdot)$ are the principle branch of the Lambert-W function and the modified Bessel function of the first kind and order zero, respectively. The simulation parameters are summarized in Table I. All numerical results are averaged over 1000 random channel realizations.

B. Complexity Analysis

First, we study the complexities of the proposed algorithms. In Fig. 4, as a measure for complexity, we compare

TABLE I
SIMULATION PARAMETERS

EH model in (2)	$\varphi_k(\|z\|^2) = \lambda\left[\mu^{-1}W_0\left(\mu\exp(\mu)I_0\left(\nu\sqrt{2\|z\|^2}\right)-1\right)^2\right],\ \forall k$		
Parameters of EH model	$\mu = 0.03,\ \nu = 2.4\cdot 10^3,$ $\lambda = 10^{-10},\ A_k^2 = 0.4\,\text{mW}, \forall k$	Grid sizes for Algorithm 1	$L_\mu = 10$ $L_\tau = 100$
Distance	In Fig. 4: $d_k = 3\,\text{m},\ \forall k$ In Fig. 5: $d_1 = 3\,\text{m}, d_2 = 5\,\text{m}, d_3 = 7\,\text{m}$ In Fig. 6: $d_k \in [3\,\text{m}, 10\,\text{m}],\ \forall k$	Grid size for Algorithm 3 Initial energy	$L_\tau = 100$ $q_k = 0\,\text{J},\ \forall k$

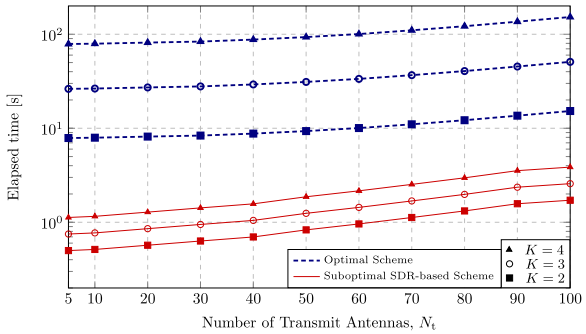

Fig. 4. Computation times of the optimal scheme and the suboptimal SDR-based design for different values of N_t and K.

the times required to determine the energy signals for the optimal scheme and the suboptimal SDR-based scheme. For the simulations, we adopt $p_k^{\text{req}} = 0\text{W}$ and the required per-user data rate is selected randomly from the interval $R_k \in [1,5]\frac{\text{bit}}{channel\ use}, \forall k$. We note that the times required to obtain the optimal and suboptimal WPCN designs depicted in Fig. 4 are proportional to the computational complexity orders Θ_{Opt} and Θ_{SDR} in (22) and (28), respectively. Thus, as expected, we observe in Fig. 4 that the computation times of both considered schemes grow with the number of users K and the number of BS antennas N_t. Furthermore, we note that for any value of K, the suboptimal SDR-based scheme entails a significantly lower complexity than the optimal WPCN design and the complexity gap between the schemes increases with the number of users K. This is due to the exponential complexity of the optimal resource allocation Θ_{RA} in K, whereas, for the SDR-based scheme, the resource allocation is obtained with the low-complexity MRT-based approach, and thus, the complexity Θ_{SDR} is significantly lower than that of the optimal solution. Moreover, although the computational complexity of the optimal and suboptimal SDR-based WPCN designs may be high for large values of N_t, we note that in this case, both schemes may not provide substantial gains over the suboptimal MRT-based scheme which is optimal for massive MISO WPCNs with vanishing system loads and whose computational complexity is very small.

C. Performance Analysis

In the following, we analyze the performances of the proposed energy signal designs for WPCNs. To this end, in Figs. 5(a) and 5(b), we compare the average transmit powers P_{DL} obtained for different numbers of users K as functions of the required per-user power, $p^{\text{req}} = p_k^{\text{req}},\ \forall k$, and the required per-user rate, $R^{\text{req}} = R_k^{\text{req}},\ \forall k$, respectively. We adopt $N_t = 5$ antennas at the BS and consider WPCNs with $K = 1$, $K = 2$, and $K = 3$ user devices. We set the distances between the BS and user devices to $d_1 = 3\text{M}$, $d_2 = 5\text{M}$, and $d_3 = 7\text{M}$, respectively. Furthermore, for the results in Figs. 5(a) and 5(a)(b), we adopt $R_k^{\text{req}} = 0\frac{\text{bit}}{channel\ use}$ and $p_k^{\text{req}} = 0\text{W}, \forall k$, respectively.

As Baseline Scheme 1 and Baseline Scheme 2, we adopt the WPCN design obtained by solving optimization problem (7) with the linear and sigmoidal EH models at the user devices, utilizing the algorithms reported in [7] and [16], respectively. For the linear EH model in Baseline Scheme 1, we adopt energy conversion efficiency $\eta_k = \frac{\phi_k(A_k^2)}{A_k^2}, \forall k$, whereas for the sigmoidal model in Baseline Scheme 2, we determine the model parameters to accurately match the adopted function $\phi_k(\cdot), \forall k$, as proposed in [14]. We note that since both baseline EH models are designed to characterize the average harvested power at the user devices, the related signal designs provide covariance matrices $\tilde{\boldsymbol{X}} = \sum \frac{\tau_n}{\tau}\boldsymbol{x}_n\boldsymbol{x}_n^H$ and assume Gaussian energy signal vectors $\boldsymbol{x}_n$. Therefore, as in [7], for the baseline schemes, we could adopt $\tilde{N} = \text{rank}\{\tilde{\boldsymbol{X}}\}$ transmit symbols vectors that are obtained from the $\tilde{N}$ dominant eigenvectors of $\tilde{\boldsymbol{X}}$. However, in our extensive simulations, we always observed $\text{rank}\{\tilde{\boldsymbol{X}}\} = 1$ and, thus, for both baseline schemes, we adopt a single transmit vector in the downlink $\boldsymbol{x}_1 = \tilde{\lambda}_1\tilde{\boldsymbol{v}}_1$, where $\tilde{\lambda}_1$ and $\tilde{\boldsymbol{v}}_1$ are the non-zero eigenvalue and the corresponding eigenvector of $\tilde{\boldsymbol{X}}$, respectively. Furthermore, since the baseline schemes may not be able to provide the required harvested powers and uplink rates if the circuit-based EH model in Table I is adopted, for the baseline schemes, we plot in Figs. 5(a) and 5(b) the average transmit powers for the achieved harvested powers and user rates, respectively.

First, we observe in Figs. 5(a) and 5(b) that for any number of users K, the average transmit power P_{DL} in the downlink increases with the required power p^{req} and the required rate R^{req}. Next, as expected, we observe that, for single-user WPCNs with $K = 1$, all proposed schemes show identical performance since the suboptimal MRT-based scheme coincides with the optimal solution in this case. We note that due to the saturation of the EH circuits, the achievable harvested power in Fig. 5(a) and the uplink information rate in Fig. 5(b) are upper bounded. Furthermore, since ZF is adopted at the BS to mitigate inter-user interference, the upper bounds in Fig. 5(b) are lower for larger numbers of users K. In Figs. 5(a) and 5(b), we observe that all proposed schemes require a lower transmit power than the baseline schemes for all considered values of K, p^{req}, and R^{req}, respectively. This is achieved by a more accurate modelling of the EH circuits for characterizing the instantaneous powers harvested at the user devices, which enables an optimal design of the downlink energy signal at the BS. Furthermore, for the maximum achievable harvested

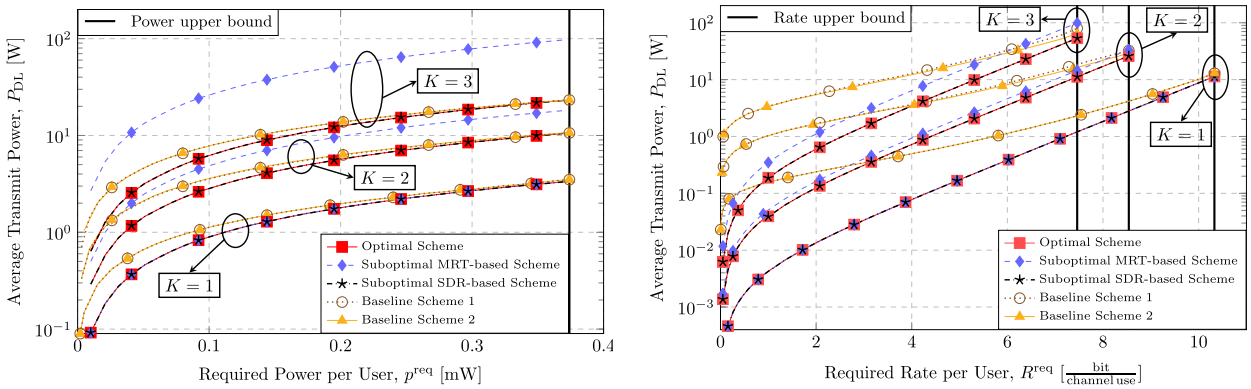

(a) Comparison for different per-user required powers p^{req}

(b) Comparison for different per-user required rates R^{req}

Fig. 5. Average transmit powers P_{DL} for different values of per-user required powers p^{req} and rates R^{req}.

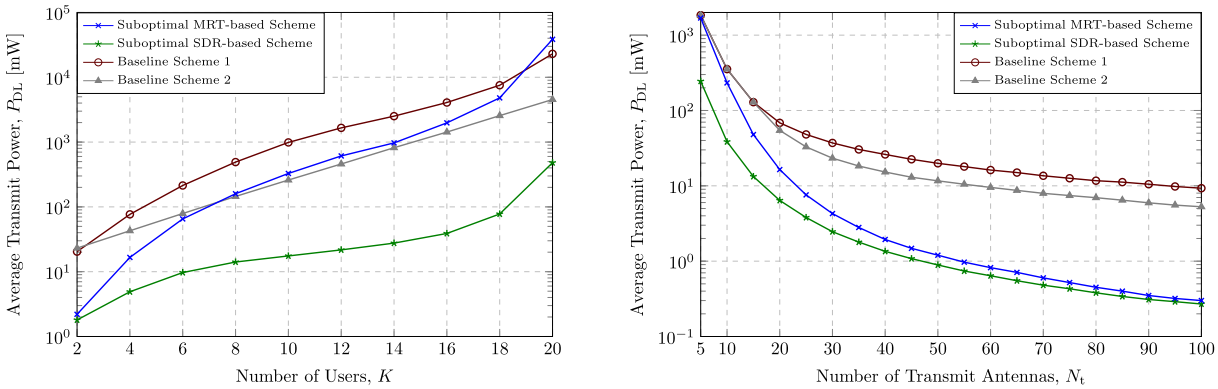

(a) Comparison for different numbers of users K

(b) Comparison for different numbers of antennas N_{t}

Fig. 6. Average transmit powers P_{DL} for different numbers of BS antennas N_{t} and users K.

powers and uplink information rates in Figs. 5(a) and 5(b), respectively, the performance gaps between the optimal and the baseline schemes are small since, in this limiting saturation regime, the optimal energy signal and resource allocation policy are determined by the weakest user, and thus, a lower number of energy beamforming vectors may be optimal in the downlink. Finally, although the suboptimal SDR-based scheme typically requires lower computational complexity than the optimal scheme, cf. Fig. 4, we observe that the performances achieved by both schemes are practically identical for all considered p^{req} and R_k^{req}.

In Figs. 6(a) and 6(b), we depict the average transmit powers as functions of the numbers of users K and BS antennas N_{t}, respectively. We adopt $p_k^{\mathrm{req}} = 0\mathrm{W}$, $R_k^{\mathrm{req}} = 3\frac{\mathrm{bit}}{channel\,use}, \forall k$, and d_k is taken randomly from the interval $d_k \in [3\mathrm{M}, 10\mathrm{M}], \forall k$. For the results in Figs. 6(a) and 6(b), we adopt $N_{\mathrm{t}} = 20$ antennas at the BS and $K = 5$ users, respectively. Since the suboptimal SDR-based scheme has significantly lower computational complexity compared to the optimal scheme for large K, cf. Fig. 4, and both schemes achieve identical performance, cf. Fig. 5, for the results in Fig. 6, we consider the suboptimal MRT- and SDR-based schemes only.

First, in Figs. 6(a) and 6(b), we observe that the required transmit power is smaller for lower numbers of users K and larger numbers of BS antennas N_{t}, respectively. This is expected since, for a given K, a higher number of transmit antennas, i.e., a smaller ratio $\frac{K}{N_{\mathrm{t}}}$, leads to a larger beamforming gain and channel hardening, which yields better WPCN performance. Next, we note that similar to the results in Fig. 5, the suboptimal SDR-based scheme achieves a significantly better performance compared to the baseline schemes due to the more accurate EH modelling which enables the optimization of the transmit energy signal waveform. However, we observe that the suboptimal MRT-based scheme shows a poor performance and is even not able to outperform the baseline schemes if the number of deployed users is high. Interestingly, the performance gap between the proposed suboptimal schemes decreases with increasing system load and for $N_{\mathrm{t}} \gg K$, both proposed suboptimal schemes achieve nearly the same performance. In fact, the MRT-based scheme becomes optimal for massive MIMO WPCNs when $N_{\mathrm{t}} \to \infty$ and orthogonal channel vectors, i.e., $\boldsymbol{h}_i \boldsymbol{h}_j^H \to 0, \forall i \neq j$, and, thus, is more efficient for smaller system loads, i.e., ratios $\frac{K}{N_{\mathrm{t}}}$.

VI. Conclusion

In this work, we considered multi-user MISO WPCNs, where, in the downlink, the BS sent an energy signal comprising multiple energy transmit signal vectors to the users, which, in turn, harvested the received power and utilized it for information transmission in the uplink. To characterize the instantaneous power harvested at the user devices, we adopted a general non-linear EH model. Then, we formulated a non-convex optimization problem, where we jointly designed the

normalized durations of the downlink and uplink subframes and the energy signal waveform. We showed that, for a single-user WPCN, the optimal signal in the downlink comprises a single energy signal vector which is collinear with the MRT beamformer and drives the EH circuit into saturation. Then, to obtain the optimal solution for general multi-user WPCNs, we derived an optimal algorithm, whose computational complexity was exponential and polynomial in the number of users and BS antennas, respectively. Moreover, we showed that the optimal energy signal for massive MISO WPCNs with vanishing system loads employs a sequence of weighted sums of the MRT beamforming vectors of the users. Then, based on this solution, we proposed a closed-form MRT-based WPCN design, which is optimal for the massive MISO regime and suboptimal for MISO WPCNs with finite system loads. Moreover, based on this scheme, we also derived a suboptimal SDR-based design that improved the performance of the MRT-based scheme for the general case. Our simulation results revealed that the proposed suboptimal SDR-based scheme entails a lower complexity than the optimal design and both schemes achieve nearly identical performances and significantly outperform two baseline schemes based on linear and sigmoidal EH models, respectively. Moreover, we observed that the performance gap between the proposed suboptimal MRT- and SDR-based schemes is small for lightly loaded WPCNs and becomes negligible when the number of BS antennas tends to infinity.

Interesting directions for future research include, e.g., the optimal design of the transmit signal waveform for multi-antenna communication networks, where not only power but also information is transmitted to the user devices in the downlink [3], [25] and the design of WPCNs that are robust to imperfect channel estimation and hardware impairments [13], [16].

Appendix A
Proof of Proposition 1

First, we note that for any given transmit power, the received power at the user device is maximized if MRT beamforming vector $\boldsymbol{w}^*$ is adopted at the BS, i.e., $\forall \boldsymbol{x}_n \in \mathbb{C}^{N_\mathrm{t}}$, $|\boldsymbol{h}\boldsymbol{x}_n| \leq |\boldsymbol{h}\boldsymbol{w}^*\alpha_n|$, where $\alpha_n = \|\boldsymbol{x}_n\|_2$. Furthermore, since a scalar phase rotation of $\boldsymbol{x}_n$ does not influence the harvested power at the user device, the optimal energy signal vectors are given by $\boldsymbol{x}_n^* = \boldsymbol{w}^* s_n^*$, where $s_n = \alpha_n^* \exp(j\theta_n)$ are scalar symbols with arbitrary phases $\theta_n \in [0, 2\pi)$. Here, α_n^* are the optimal symbol magnitudes that solve the following optimization problem:

$$\underset{\boldsymbol{\tau}^\mathrm{d}\succeq\mathbf{0},\bar{\tau}\in[0,1],\boldsymbol{\alpha},N}{\text{minimize}} \quad \sum_{n=1}^{N} \tau_n^\mathrm{d}\alpha_n^2 \tag{29a}$$

$$\text{subject to} \quad \sum_{n=1}^{N} \tau_n^\mathrm{d}\phi(\alpha_n^2\|\boldsymbol{h}\|_2^2) \geq \xi(\bar{\tau}), \tag{29b}$$

$$\sum_{n=1}^{N} \tau_n^\mathrm{d} = \bar{\tau}, \tag{29c}$$

with $\boldsymbol{\alpha} = [\alpha_1, \alpha_2, \cdots, \alpha_N]$.

Next, we note that function $\phi(|z|^2)$ in (29) is convex for $|z| \leq A$ and upper-bounded, i.e., $\phi(|z|^2) = \phi(A^2)$, $\forall |z| \geq A$. Therefore, for any given value $\bar{\tau}$, the optimal solution[13] to problem (29) includes at most $N = 2$ energy signal vectors, whose magnitudes are $\alpha_1^* = \alpha_s^*$ and $\alpha_2 = 0$, respectively, with corresponding time lengths $\tau_1^\mathrm{d} = \frac{\xi(\bar{\tau})}{\phi(A^2)}$ and $\tau_2^\mathrm{d} = \bar{\tau} - \tau_1^\mathrm{d}$ [24], [25]. Thus, problem (29) can be further simplified as follows:

$$\underset{\bar{\tau}\in[0,1],\tau_1^\mathrm{d}\geq 0}{\text{minimize}} \quad \tau_1^\mathrm{d} \quad \text{subject to } \tau_1^\mathrm{d}\phi(A^2) \geq \xi(\bar{\tau}),\ \tau_1^\mathrm{d} \leq \bar{\tau}. \tag{30}$$

Since a larger time slot duration $\bar{\tau}$ leads to a higher power requirement $(1-\bar{\tau})p_{\min}^\mathrm{u}$ for the uplink transmission phase, function $\xi(\bar{\tau})$ in (30) is monotonic increasing. Therefore, if problem (30) is feasible, the optimal duration of the zero-valued downlink energy signal vector with $\alpha_2 = 0$ is $\tau_2^\mathrm{d} = 0$. Thus, the optimal time allocation is achieved with $\tau_1^\mathrm{d} = \bar{\tau}$ and hence, one energy signal vector $\boldsymbol{x}^*$ is utilized at the BS, i.e., $N^* = 1$. This concludes the proof.

Appendix B
Proof of Proposition 2

Let us reformulate optimization problem (11) equivalently as follows:

$$\underset{\boldsymbol{\tau}^\mathrm{d},\bar{\tau},\boldsymbol{X},\boldsymbol{M},N}{\text{minimize}} \quad \sum_{n=1}^{N} \tau_n^\mathrm{d}\|\boldsymbol{x}_n\|_2^2 \tag{31a}$$

$$\text{subject to} \quad \sum_{n=1}^{N} \tau_n^\mathrm{d} = \bar{\tau}, \tag{31b}$$

$$\sum_{n=1}^{N} \tau_n^\mathrm{d}\boldsymbol{\mu}_n \succeq \boldsymbol{\xi}^\mathrm{d}(\bar{\tau}), \tag{31c}$$

$$\phi_k\left(|\boldsymbol{h}_k\boldsymbol{x}_n|^2\right) \geq \mu_{n,k}, \forall k, \tag{31d}$$

where $\boldsymbol{M} = [\boldsymbol{\mu}_1, \boldsymbol{\mu}_2, \cdots, \boldsymbol{\mu}_N]$. Since the harvested powers at the user devices are independent of a scalar phase rotation of $\boldsymbol{x}_n, n \in \{1, 2, \cdots, N\}$, we decompose the transmit energy signal vectors as in (12). Next, we note that for any given vector of harvested powers in time slot n, $\boldsymbol{\mu}_n = [\mu_{n,1}, \mu_{n,2}, \cdots, \mu_{n,K}]^\top$, the optimal energy beamforming vector $\boldsymbol{w}_n^*$ that minimizes the instantaneous transmit power $\|\boldsymbol{w}_n\|_2^2$ and yields $\boldsymbol{\mu}_n$ can be obtained as in (13) and the corresponding minimum transmit power is given by $\psi(\boldsymbol{\mu}_n)$. Finally, since for the optimal $\boldsymbol{x}_n^*$ and $\boldsymbol{\mu}_n^*$, we have $\|\boldsymbol{x}_n^*\|_2^2 = \psi(\boldsymbol{\mu}_n^*)$, problem (31) can be equivalently reformulated as (14). This concludes the proof.

Appendix C
Proof of Proposition 3

Since $\phi_k(\cdot)$ is monotonic non-decreasing and is given by (2), optimization problem (15) can be equivalently reformulated as follows:

$$\psi(\boldsymbol{\mu}) = \min_{\boldsymbol{X}\in\Omega_\mathcal{S}(\boldsymbol{\mu})} \mathrm{Tr}\{\boldsymbol{X}\} \tag{32}$$

with $\Omega_\mathcal{S}(\boldsymbol{\mu}) = \{\boldsymbol{X} : \boldsymbol{h}_k\boldsymbol{X}\boldsymbol{h}_k^H \geq \phi_k^{-1}(\mu_k), k \in \{1, 2, \cdots, K\}, \forall k, \boldsymbol{X} \in \mathcal{S}_+^{N_\mathrm{t}}, \mathrm{rank}\{\boldsymbol{X}\} \leq 1\}$, where

[13]The corresponding proof is similar to that of [24, Corollary 3] and is omitted here due to space constraints.

$\boldsymbol{X} = \boldsymbol{x}\boldsymbol{x}^H$. Furthermore, the matrix $\boldsymbol{X}^*$ that solves the following problem:

$$\underset{\boldsymbol{X}\in\mathcal{S}_+^{N_\mathrm{t}}}{\text{minimize}} \quad \mathrm{Tr}\{\boldsymbol{X}\} \tag{33a}$$

$$\text{subject to} \quad \boldsymbol{h}_k\boldsymbol{X}\boldsymbol{h}_k^H \geq \phi_k^{-1}(\mu_k), \forall k, \tag{33b}$$

satisfies $\mathrm{rank}\{\boldsymbol{X}^*\} \leq 1$, cf. Lemma 1 in Section III-C.3. Hence, the value of function $\psi(\boldsymbol{\mu})$ can be equivalently obtained as $\psi(\boldsymbol{\mu}) = \mathrm{Tr}\{\boldsymbol{X}^*\}$, where $\boldsymbol{X}^*$ is the solution of problem (33).

Let us consider optimization problem (33). We note that (33) is a convex problem and, hence, its solution entails a computational complexity that is polynomial in N_t [32]. Since we have $N_\mathrm{t} \geq K$, to reduce the complexity of determining $\psi(\boldsymbol{\mu})$, in the following, we consider the dual problem associated with optimization problem (33) and given by

$$\underset{\boldsymbol{\lambda}\succeq\boldsymbol{0}}{\text{maximize}} \quad \boldsymbol{\rho}^\top\boldsymbol{\lambda} \tag{34a}$$

$$\text{subject to} \quad \boldsymbol{I} - \sum_{k=1}^{K}\boldsymbol{h}_k^H\boldsymbol{h}_k\lambda_k \in \mathcal{S}_+^{N_\mathrm{t}}, \tag{34b}$$

where $\rho_k = \varphi_k^{-1}(\mu_k)$ and $\boldsymbol{\lambda} \in \mathbb{R}^K$ is a vector of Lagrangian multipliers associated with the constraints in (33). Since problem (33) is convex and satisfies Slater's conditions, the duality gap is zero and the solutions $\boldsymbol{X}^*$ and $\boldsymbol{\lambda}^*$ satisfy $\psi(\boldsymbol{\mu}) = \mathrm{Tr}\{\boldsymbol{X}^*\} = \boldsymbol{\rho}^\top\boldsymbol{\lambda}^*$.

Finally, we consider the constraint in (34). We note that the constraint is satisfied if and only if all the eigenvalues of matrix $\boldsymbol{I} - \boldsymbol{H}^H\boldsymbol{\Lambda}\boldsymbol{H}$, where $\boldsymbol{\Lambda} = \mathrm{diag}\{\boldsymbol{\lambda}\}$, are non-negative, i.e., $\|\boldsymbol{H}^H\boldsymbol{\Lambda}\boldsymbol{H}\|_2 \leq 1$. Furthermore, $\|\boldsymbol{H}^H\boldsymbol{\Lambda}\boldsymbol{H}\|_2 = \sqrt{\lambda_{\max}\big(\boldsymbol{\Sigma}\boldsymbol{U}^H\boldsymbol{\Lambda}\boldsymbol{U}\boldsymbol{\Sigma}^2\boldsymbol{U}^H\boldsymbol{\Lambda}\boldsymbol{U}\boldsymbol{\Sigma}\big)} = \sqrt{\lambda_{\max}\big(\boldsymbol{U}\boldsymbol{\Sigma}^2\boldsymbol{U}^H\boldsymbol{\Lambda}\boldsymbol{U}\boldsymbol{\Sigma}^2\boldsymbol{U}^H\boldsymbol{\Lambda}\big)} = \|\boldsymbol{B}\boldsymbol{\Lambda}\boldsymbol{B}\|_2$, where $\boldsymbol{H} = \boldsymbol{U}\boldsymbol{\Sigma}\boldsymbol{V}^H$ is the singular value decomposition of $\boldsymbol{H}$ and $\lambda_{\max}(\boldsymbol{A})$ denotes the largest eigenvalue of $\boldsymbol{A}$. Hence, the constraint in (34) is equivalent to $\|\boldsymbol{B}\boldsymbol{\Lambda}\boldsymbol{B}\|_2 \leq 1$. This concludes the proof.

Appendix D
Proof of Proposition 4

For any given $\bar{\tau}$, N, and set of vectors $\boldsymbol{\mu}_n, n \in \{1, 2, \cdots, N\}$, optimization problem (14) is linear in $\boldsymbol{\tau}$ and involves N variables and $K+1$ constraints. We note that the solution of a linear optimization problem with $\tilde{N}$ variables and $\tilde{K} \leq \tilde{N}$ constraints is a vertex of the polytope defined by the $\tilde{K}$ constraints, and thus, the corresponding vector determining the solution of the linear problem has at most $\tilde{K}$ non-zero elements [32]. Thus, for the optimal solution of (14) and, hence, (11) and (7), at most $N^* = K+1$ time slots have non-zero lengths. This concludes the proof.

Appendix E
Proof of Lemma 1

The proof below follows along the lines of the proof in [36, Appendix C]. Since problem (19) is convex and Slater's conditions are satisfied, strong duality holds and the gap between problem (19) and its dual problem is equal to zero [37]. We express the Lagrangian of (19) as follows:

$$\mathcal{L}(\boldsymbol{X}) = \mathrm{Tr}\{\boldsymbol{X}\} - \sum_{k=1}^{K}\gamma_k\boldsymbol{h}_k\boldsymbol{X}\boldsymbol{h}_k^H - \boldsymbol{Y}\boldsymbol{X} + \bar{\gamma}, \tag{35}$$

where $\gamma_k, k \in \{1, 2, \cdots, K\}$, are the Lagrangian multipliers associated with the K constraints of problem (19) and $\bar{\gamma}$ collects all terms that do not depend on $\boldsymbol{X}$. Here, $\boldsymbol{Y}$ is the Lagrangian multiplier associated with constraint $\boldsymbol{X} \in \mathcal{S}_+^{N_\mathrm{t}}$. We note that the Karush-Kuhn-Tucker (KKT) conditions are satisfied for the optimal solution $\boldsymbol{X}^*$ of (19) and the solutions $\gamma_k^*, k \in \{1, 2, \cdots, K\}$, and $\boldsymbol{Y}^*$ of the corresponding dual problem. The KKT conditions are given by [38]

$$\nabla\mathcal{L}(\boldsymbol{X}^*) = \boldsymbol{0}_{N_\mathrm{t}\times N_\mathrm{t}} \tag{36a}$$

$$\boldsymbol{Y}^* \succeq \boldsymbol{0}_{N_\mathrm{t}\times N_\mathrm{t}}, \gamma_k^* \geq 0, \forall k \tag{36b}$$

$$\boldsymbol{Y}^*\boldsymbol{X}^* = \boldsymbol{0}_{N_\mathrm{t}\times N_\mathrm{t}}, \tag{36c}$$

where $\boldsymbol{0}_{N_\mathrm{t}\times N_\mathrm{t}}$ stands for the all-zero matrix of size $N_\mathrm{t} \times N_\mathrm{t}$ and $\nabla\mathcal{L}(\boldsymbol{X}^*)$ denotes the gradient of $\mathcal{L}(\boldsymbol{X})$ evaluated at $\boldsymbol{X}^*$. Next, we express condition (36a) as follows

$$\boldsymbol{Y}^* = \boldsymbol{I}_{N_\mathrm{t}} - \boldsymbol{\Delta}, \tag{37}$$

where $\boldsymbol{\Delta} = \sum_k \gamma_k^*\boldsymbol{h}_k^H\boldsymbol{h}_k$. Let us now investigate the structure of $\boldsymbol{\Delta}$. We denote the maximum eigenvalue of $\boldsymbol{\Delta}$ by $\delta^{\max} \in \mathbb{R}$. Due to the randomness of the channel, with probability 1, only one eigenvalue of $\boldsymbol{\Delta}$ has value[14] $\delta^{\max}$ [39]. Considering (37), we note that if $\delta^{\max} < 1$, then $\boldsymbol{Y}^*$ is a full-rank positive definite matrix. In this case, (36c) yields $\boldsymbol{X}^* = \boldsymbol{0}_{N_\mathrm{t}\times N_\mathrm{t}}$, and hence, $\mathrm{rank}\{\boldsymbol{X}^*\} = 0$. Furthermore, if $\delta^{\max} > 1$, then $\boldsymbol{Y}^*$ is not a positive semidefinite matrix, which contradicts (36b). Finally, if $\delta^{\max} = 1$, then $\boldsymbol{Y}^*$ is a positive semidefinite matrix with $\mathrm{rank}\{\boldsymbol{Y}^*\} = N_\mathrm{t} - 1$. Then, applying Sylvester's rank inequality to (36c), we have

$$0 = \mathrm{rank}\{\boldsymbol{Y}^*\boldsymbol{X}^*\} \geq \mathrm{rank}\{\boldsymbol{Y}^*\} + \mathrm{rank}\{\boldsymbol{X}^*\} - N_\mathrm{t} = \mathrm{rank}\{\boldsymbol{X}^*\} - 1. \tag{38}$$

Thus, we have $\mathrm{rank}\{\boldsymbol{X}^*\} \leq 1$. This concludes the proof.

Appendix F
Proof of Proposition 6

Since $\boldsymbol{h}_i\boldsymbol{h}_j^H = 0, \forall i \neq j$, matrix $\boldsymbol{B}$ in Proposition 3 is diagonal and the solution of problem (16) is given by $\lambda_k = \frac{1}{\|\boldsymbol{h}_k\|_2^2}, k \in \{1, 2, \cdots, K\}$. Hence, the corresponding instantaneous transmit power can be obtained as $\psi(\boldsymbol{\mu}) = \sum_{k=1}^{K}\varphi_k^{-1}(\mu_k)\frac{1}{\|\boldsymbol{h}_k\|_2^2}$. Thus, we note that, for the optimal downlink energy signal, the channel $\boldsymbol{H}$ between the BS and the user devices can be equivalently decomposed into K parallel independent subchannels $\boldsymbol{h}_k, k \in \{1, 2, \cdots, K\}$, and the power harvested at user device k in time slot n does not depend on the powers harvested at the other devices. Furthermore, similarly, the optimal average transmit power in the downlink for energy transmission to user k is independent of the powers transmitted to the

[14] In our exhaustive simulations, we have always observed that only one eigenvalue of matrix $\boldsymbol{\Delta}$ has value $\delta^{\max}$.

other users. Thus, the optimal average transmit power in (23) can be expressed as $P^*_{\mathrm{DL}}(\bar{\tau}) = \sum_{n=1}^{\bar{N}} \tau_n^{\mathrm{d}*} \psi(\boldsymbol{\mu}_n^*) = \sum_{k=1}^{K} \sum_{n=1}^{\bar{N}} \bar{\tau}_n^{\mathrm{d}*} \varphi_k^{-1}(\mu_{n,k}^*) \frac{1}{\|\boldsymbol{h}_k\|_2^2} = \sum_{k=1}^{K} \frac{1}{\|\boldsymbol{h}_k\|_2^2} P^*_{\mathrm{DL},k}(\bar{\tau})$, where $P^*_{\mathrm{DL},k}(\bar{\tau}) = \sum_{n=1}^{N_k^*} \tilde{\tau}_{n,k}^{\mathrm{d}*} \varphi_k^{-1}(\mu_{n,k}^*)$ is the normalized optimal downlink average transmit power for energy transfer to user k. Here, $\tilde{\tau}_{n,k}^{\mathrm{d}*}$ and N_k^* are the duration of the time slot, where user k harvests power $\mu_{n,k}^*$, $n \in \{1, 2, \cdots, N_k^*\}, k \in \{1, 2, \cdots, K\}$, and the optimal number of time slots for user k, respectively.

To determine $N_k^*, \tilde{\tau}_{n,k}^{\mathrm{d}*}$, and $\mu_{n,k}^*, n \in \{1, 2, \cdots, N_k^*\}, k \in \{1, 2, \cdots, K\}$, we equivalently decompose problem (14) into K subproblems, where subproblem $k, k \in \{1, 2, \cdots, K\}$, defines the optimal resource allocation for user k, and formulate the subproblem for user k as follows:

$$\underset{\tilde{\boldsymbol{\tau}}_k^{\mathrm{d}} \succeq \mathbf{0}, \tilde{\boldsymbol{\mu}}_k, N_k}{\text{minimize}} \quad \sum_{n=1}^{N_k} \tilde{\tau}_{n,k}^{\mathrm{d}} \varphi_k^{-1}(\mu_{n,k}) \tag{39a}$$

$$\text{subject to} \quad \sum_{n=1}^{N_k} \tilde{\tau}_{n,k}^{\mathrm{d}} \mu_{n,k} \geq \xi_k^{\mathrm{d}}(\bar{\tau}), \tag{39b}$$

$$\sum_{n=1}^{N_k} \tilde{\tau}_{n,k}^{\mathrm{d}} = \bar{\tau}, \tag{39c}$$

where $\tilde{\boldsymbol{\tau}}_k^{\mathrm{d}} = [\tilde{\tau}_{1,k}^{\mathrm{d}}, \tilde{\tau}_{2,k}^{\mathrm{d}}, \cdots, \tilde{\tau}_{N_k,k}^{\mathrm{d}}]$ and $\tilde{\boldsymbol{\mu}}_k = [\mu_{1,k}, \mu_{2,k}, \cdots, \mu_{N_k,k}]$. Similar to the single-user WPCN in Proposition 1, at most $\bar{N}_k = 2$ time slots are needed for problem (39). The optimal harvested powers and the durations of the corresponding time slots are given by $\mu_{1,k}^* = \phi_k(A_k^2)$, $\mu_{2,k}^* = 0$ and $\tilde{\tau}_{1,k}^{\mathrm{d}} = \frac{\xi_k^{\mathrm{d}}(\bar{\tau})}{\phi_k(A_k^2)}$, $\tilde{\tau}_{2,k}^{\mathrm{d}} = \bar{\tau} - \tilde{\tau}_{1,k}^{\mathrm{d}}$, respectively. Hence, the optimal average transmit power in (23) is given by $P^*_{\mathrm{DL}}(\bar{\tau}) = \sum_{k=1}^{K} \frac{A_k^2}{\|\boldsymbol{h}_k\|_2^2} \frac{\xi_k^{\mathrm{d}}(\bar{\tau})}{\phi_k(A_k^2)}$. We note that the downlink transmit policy in Proposition 6 yields the optimal transmit power $P^*_{\mathrm{DL}}(\bar{\tau})$ and satisfies the constraints in (39). Hence, for a given $\bar{\tau}$, the energy beamforming vectors and time slot durations in (25) are the solution of (11). This concludes the proof.

REFERENCES

[1] N. Shanin, M. Garkisch, A. Hagelauer, R. Schober, and L. Cottatellucci, "Optimal resource allocation and beamforming for two-user MISO WPCNs for a non-linear circuit-based EH model," in *Proc. IEEE Int. Conf. Acoust., Speech Signal Process. (ICASSP)*, May 2022, pp. 8642–8646.

[2] S. Bi, C. K. Ho, and R. Zhang, "Wireless powered communication: Opportunities and challenges," *IEEE Commun. Mag.*, vol. 53, no. 4, pp. 117–125, Apr. 2015.

[3] B. Clerckx, R. Zhang, R. Schober, D. W. K. Ng, D. I. Kim, and H. V. Poor, "Fundamentals of wireless information and power transfer: From RF energy harvester models to signal and system designs," *IEEE J. Sel. Areas Commun.*, vol. 37, no. 1, pp. 4–33, Jan. 2019.

[4] Z. Wei, X. Yu, D. W. K. Ng, and R. Schober, "Resource allocation for simultaneous wireless information and power transfer systems: A tutorial overview," *Proc. IEEE*, vol. 110, no. 1, pp. 127–149, Jan. 2022.

[5] H. Tataria, M. Shafi, A. F. Molisch, M. Dohler, H. Sjöland, and F. Tufvesson, "6G wireless systems: Vision, requirements, challenges, insights, and opportunities," *Proc. IEEE*, vol. 109, no. 7, pp. 1166–1199, Jul. 2021.

[6] H. Ju and R. Zhang, "Throughput maximization in wireless powered communication networks," *IEEE Trans. Wireless Commun.*, vol. 13, no. 1, pp. 418–428, Jan. 2014.

[7] L. Liu, R. Zhang, and K.-C. Chua, "Multi-antenna wireless powered communication with energy beamforming," *IEEE Trans. Commun.*, vol. 62, no. 12, pp. 4349–4361, Dec. 2014.

[8] G. Yang, C. K. Ho, R. Zhang, and Y. L. Guan, "Throughput optimization for massive MIMO systems powered by wireless energy transfer," *IEEE J. Sel. Areas Commun.*, vol. 33, no. 8, pp. 1640–1650, Jan. 2015.

[9] H. Lee, K.-J. Lee, H. Kim, B. Clercks, and I. Lee, "Resource allocation techniques for wireless powered communication networks with energy storage constraint," *IEEE Trans. Wireless Commun.*, vol. 15, no. 4, pp. 2619–2628, Apr. 2016.

[10] R. Morsi, D. S. Michalopoulos, and R. Schober, "Performance analysis of near-optimal energy buffer aided wireless powered communication," *IEEE Trans. Wireless Commun.*, vol. 17, no. 2, pp. 863–881, Feb. 2018.

[11] X. Gu, S. Hemour, and K. Wu, "Far-field wireless power harvesting: Nonlinear modeling, rectenna design, and emerging applications," *Proc. IEEE*, vol. 110, no. 1, pp. 56–73, Jan. 2022.

[12] U. Tietze and C. Schenk, *Advanced Electronic Circuits*. Berlin, Germany: Springer, 2012.

[13] N. Shanin, L. Cottatellucci, and R. Schober, "Markov decision process based design of SWIPT systems: Non-linear EH circuits, memory, and impedance mismatch," *IEEE Trans. Commun.*, vol. 69, no. 2, pp. 1259–1274, Feb. 2021.

[14] E. Boshkovska, D. W. K. Ng, N. Zlatanov, and R. Schober, "Practical non-linear energy harvesting model and resource allocation for SWIPT systems," *IEEE Commun. Lett.*, vol. 19, no. 12, pp. 2082–2085, Sep. 2015.

[15] E. Boshkovska, D. W. K. Ng, N. Zlatanov, A. Koelpin, and R. Schober, "Robust resource allocation for MIMO wireless powered communication networks based on a non-linear EH model," *IEEE Trans. Commun.*, vol. 65, no. 5, pp. 1984–1999, May 2017.

[16] E. Boshkovska, D. W. K. Ng, L. Dai, and R. Schober, "Power-efficient and secure WPCNs with hardware impairments and non-linear EH circuit," *IEEE Trans. Commun.*, vol. 66, no. 6, pp. 2642–2657, Jun. 2018.

[17] M. Hua, Q. Wu, and H. Vincent Poor, "Power-efficient passive beamforming and resource allocation for IRS-aided WPCNs," *IEEE Trans. Commun.*, vol. 70, no. 5, pp. 3250–3265, May 2022.

[18] P. Zeng, Q. Wu, and D. Qiao, "Energy minimization for IRS-aided WPCNs with non-linear energy harvesting model," *IEEE Wireless Commun. Lett.*, vol. 10, no. 11, pp. 2592–2596, Nov. 2021.

[19] Z. Li, W. Chen, Q. Wu, H. Cao, K. Wang, and J. Li, "Robust beamforming design and time allocation for IRS-assisted wireless powered communication networks," *IEEE Trans. Commun.*, vol. 70, no. 4, pp. 2838–2852, Apr. 2022.

[20] B. Clerckx, E. Bayguzina, D. Yates, and P. D. Mitcheson, "Waveform optimization for wireless power transfer with nonlinear energy harvester modeling," in *Proc. Int. Symp. Wireless Commun. Syst. (ISWCS)*, Aug. 2015, pp. 276–280.

[21] B. Clerckx, "Wireless information and power transfer: Nonlinearity, waveform design, and rate-energy tradeoff," *IEEE Trans. Signal Process.*, vol. 66, no. 4, pp. 847–862, Feb. 2018.

[22] B. Clerckx, Z. B. Zawawi, and K. Huang, "Wirelessly powered backscatter communications: Waveform design and SNR-energy tradeoff," *IEEE Commun. Lett.*, vol. 21, no. 10, pp. 2234–2237, Oct. 2017.

[23] Z. B. Zawawi, Y. Huang, and B. Clerckx, "Multiuser wirelessly powered backscatter communications: Nonlinearity, waveform design, and SINR-energy tradeoff," *IEEE Trans. Wireless Commun.*, vol. 18, no. 1, pp. 241–253, Jan. 2019.

[24] N. Shanin, L. Cottatellucci, and R. Schober, "Optimal transmit strategy for multi-user MIMO WPT systems with non-linear energy harvesters," *IEEE Trans. Commun.*, vol. 70, no. 3, pp. 1726–1741, Mar. 2022.

[25] R. Morsi, V. Jamali, A. Hagelauer, D. W. K. Ng, and R. Schober, "Conditional capacity and transmit signal design for SWIPT systems with multiple nonlinear energy harvesting receivers," *IEEE Trans. Commun.*, vol. 68, no. 1, pp. 582–601, Jan. 2020.

[26] S. Jaeckel, L. Raschkowski, K. Börner, and L. Thiele, "QuaDRiGa: A 3-D multi-cell channel model with time evolution for enabling virtual field trials," *IEEE Trans. Antennas Propag.*, vol. 62, no. 6, pp. 3242–3256, Jun. 2014.

[27] L. Lu, G. Y. Li, A. L. Swindlehurst, A. Ashikhmin, and R. Zhang, "An overview of massive MIMO: Benefits and challenges," *IEEE J. Sel. Topics Signal Process.*, vol. 8, no. 5, pp. 742–758, Jun. 2014.

[28] S. Vishwanath, N. Jindal, and A. Goldsmith, "Duality, achievable rates, and sum-rate capacity of Gaussian MIMO broadcast channels," *IEEE Trans. Inf. Theory*, vol. 49, no. 10, pp. 2658–2668, Oct. 2003.

[29] G. Interdonato, M. Karlsson, E. Bjornson, and E. G. Larsson, "Local partial zero-forcing precoding for cell-free massive MIMO," *IEEE Trans. Wireless Commun.*, vol. 19, no. 7, pp. 4758–4774, Jul. 2020.

[30] D. Tse and P. Viswanath, *Fundamentals Wireless Commun.*. Cambridge, U.K.: Cambridge Univ. Press, 2005.

[31] M. Grant and S. Boyd. (2015). *CVX: MATLAB Software for Disciplined Convex Programming, Version 2.0 Beta (2013)*. [Online]. Available: http://cvxr.com/cvx

[32] I. Pólik and T. Terlaky, *Interior Point Methods for Nonlinear Optimization*. Berlin, Germany: Springer, 2010.

[33] I. D. Coope and C. J. Price, "On the convergence of grid-based methods for unconstrained optimization," *SIAM J. Optim.*, vol. 11, no. 4, pp. 859–869, Jan. 2001.

[34] E. Björnson, G. Zheng, M. Bengtsson, and B. Ottersten, "Robust monotonic optimization framework for multicell MISO systems," *IEEE Trans. Signal Process.*, vol. 60, no. 5, pp. 2508–2523, May 2012.

[35] A. Zappone, E. Björnson, L. Sanguinetti, and E. Jorswieck, "Globally optimal energy-efficient power control and receiver design in wireless networks," *IEEE Trans. Signal Process.*, vol. 65, no. 11, pp. 2844–2859, Jun. 2017.

[36] N. Shanin, L. Cottatellucci, and R. Schober, "Optimal transmit strategy for MIMO WPT systems with non-linear energy harvesting," in *Proc. 17th Int. Conf. Distrib. Comput. Sensor Syst. (DCOSS)*, Jul. 2021, pp. 520–527.

[37] S. Boyd, S. P. Boyd, and L. Vandenberghe, *Convex Optimization*. Cambridge, U.K.: Cambridge Univ. Press, 2004.

[38] Z.-Q. Luo and T.-H. Chang, "SDP relaxation of homogeneous quadratic optimization: Approximation bounds and applications," in *Convex Optimization in Signal Processing and Communications*, D. P. Palomar and Y. C. Eldar, Eds. Cambridge, U.K.: Cambridge Univ. Press, 2009, pp. 117–165.

[39] D. Xu, X. Yu, Y. Sun, D. W. K. Ng, and R. Schober, "Resource allocation for secure IRS-assisted multiuser MISO systems," in *Proc. IEEE Globecom Workshops (GC Wkshps)*, Dec. 2019, pp. 1–6.

Nikita Shanin (Graduate Student Member, IEEE) received the Diploma degree (Hons.) in electrical engineering from Bauman Moscow State Technical University (BMSTU), Moscow, Russia, in 2018. He is currently pursuing the Ph.D. degree with the Institute for Digital Communications, Friedrich-Alexander Universität (FAU) Erlangen-Nürnberg, Germany. His research interests include broad areas of statistical signal processing and wireless communications, wireless information, and power transfer.

Amelie Hagelauer (Senior Member, IEEE) received the Dipl.-Ing. degree in mechatronics and the Dr.-Ing. degree in electrical engineering from the FAU Erlangen-Nuremberg, Germany, in 2007 and 2013, respectively. In November 2007, she joined the FAU Institute for Electronics Engineering, where she researched on BAW resonators and filters toward her Ph.D. degree. Since 2013, she has been focusing on SAW/BAW and RF MEMS components, as well as on microwave integrated circuits for frontends. From 2016 to 2019, she was leading a Research Group on electronic circuits. From August 2019 to September 2021, she was a Full Professor with the University of Bayreuth, Germany. In September 2021, she joined the Technical University of Munich (TUM) as a Full Professor and became the Co-Director of the Fraunhofer Institute for Electronic Microsystems and Solid State Technologies EMFT, Munich. She has authored or coauthored more than 150 peer-reviewed publications in her research fields, which include research and development of microwave theory and technology, electronic circuits and systems, and communication and sensing systems. She acted as a Guest Editor for a special issue of the IEEE TRANSACTIONS ON MICROWAVE THEORY AND TECHNIQUES on the topic RF Frontends for Mobile Radio and an Associate Editor of the IEEE TRANSACTIONS ON MICROWAVE THEORY AND TECHNIQUES.

Laura Cottatellucci (Member, IEEE) received the M.Sc. degree in electrical engineering from La Sapienza University, Rome, Italy, the Ph.D. degree from the Technical University of Vienna, Austria, in 2006, and the Habilitation degree from the University of Nice-Sophia Antipolis, France. Since December 2017, she has been a Professor of digital communications with Friedrich Alexander Universität (FAU) Erlangen-Nürnberg, Germany, and an Adjunct Professor with EURECOM, France, since September 2021. She worked for Telecom Italia for five years and as a Senior Researcher with Forschungszentrum Telekommunikation Wien, Austria (April 2000–September 2005). She was a Research Fellow with INRIA, France, from October 2005–December 2005; and the University of South Australia in 2006. From December 2006 to November 2017, she was an Assistant Professor with EURECOM, where she was also an Adjunct Professor from March 2018 to August 2019. Her research interests include communications theory and signal processing for wireless communications, satellite, and complex networks. She was an Elected Member of the IEEE Technical Committee on Signal Processing for Communications and Networking (2017–2022). She served as an Associate Editor for the IEEE TRANSACTIONS ON COMMUNICATIONS from September 2015 to August 2020 and the IEEE TRANSACTIONS ON SIGNAL PROCESSING from February 2016 to February 2020. Since September 2022, she has been Senior Member of the editorial board of *IEEE Signal Processing Magazine*.

Robert Schober (Fellow, IEEE) received the Diploma (Univ.) and Ph.D. degrees in electrical engineering from the Friedrich-Alexander University of Erlangen-Nuremberg (FAU), Germany, in 1997 and 2000, respectively.

From 2002 to 2011, he was a Professor and the Canada Research Chair with the University of British Columbia (UBC), Vancouver, Canada. Since January 2012, he has been an Alexander von Humboldt Professor and the Chair for Digital Communication with FAU. His research interests include broad areas of communication theory, wireless and molecular communications, and statistical signal processing.

Dr. Schober is a fellow of the Canadian Academy of Engineering, a fellow of the Engineering Institute of Canada, and a member of the German National Academy of Science and Engineering. He received several awards for his work including the 2002 Heinz Maier Leibnitz Award of the German Science Foundation (DFG), the 2004 Innovations Award of the Vodafone Foundation for Research in Mobile Communications, the 2006 UBC Killam Research Prize, the 2007 Wilhelm Friedrich Bessel Research Award of the Alexander von Humboldt Foundation, the 2008 Charles McDowell Award for Excellence in Research from UBC, the 2011 Alexander von Humboldt Professorship, the 2012 NSERC E. W. R. Stacie Fellowship, the 2017 Wireless Communications Recognition Award by the IEEE Wireless Communications Technical Committee, and the 2022 IEEE Vehicular Technology Society Stuart F. Meyer Memorial Award. He also received numerous best paper awards for his work including the 2022 ComSoc Stephen O. Rice Prize. Since 2017, he has been listed as a Highly Cited Researcher by the Web of Science. He served as an Editor-in-Chief for the IEEE TRANSACTIONS ON COMMUNICATIONS, VP Publications of the IEEE Communication Society (ComSoc), ComSoc Member-at-Large, and ComSoc Treasurer. He is currently serves as an Senior Editor for the Proceedings of the IEEE and ComSoc President-Elect.